1 Contents

2 Introduction

Timber has historically been a crucial structural material in underground construction, and remains so to this day. Used as temporary works, prior to the installation of permanent works such as concrete, steel, or brick (historically). Timber has many advantages over other temporary works materials such as steel. Timber has a lower density, which reduces the cost of transportation. Timber can be easily sawn and manipulated, without requiring specialist tools or permits, which makes installation more able to suit specific site requirements. In contrast, carefully dimensioned and engineered excavation is required when using (for example) steel as a temporary works material.

However, there are disadvantages associated with timber. Increasing material costs and labour costs (due to labour intensive installation) are making timber less competitive. There are, therefore, clear benefits to be found from optimizing the use of timber, to reduce material usage and therefore costs.

Presently, a significant number of safety factors are used in the design of timber in general. Many material safety factors are required to account for variables such as grain direction, moisture content, knots within the grain, and more. In addition to these material safety factors, safety factors associated with the load are applied. In underground construction, estimating this applied load can be a large problem in itself. In the hundreds of years that timber has been used in the London Underground, only one recorded case of failure exists (Mackenzie 2014). Therefore, it is considered that there is scope for in-situ investigations of the performance of timbers. It is hoped that this could lead to advances in design methods, improving the efficiency of material use, and reducing costs.

Ongoing research within CUED, known as the SmartPlank project (Xu et al. 2015), is being carried out to develop a wireless network and sensor system capable of monitoring the strain applied to timber beams in the London Underground (LU). A prototype SmartPlank system has been installed and monitored at Tottenham Court Road LU station, as part of the Crossrail project upgrades.

In the course of this report, the design methods used historically, and presently in the mining industry, and the LU, will be investigated. Comparisons will be made between data collected so far by SmartPlank and the relevant design methods. In addition, the relative performance of SmartPlank will be investigated. It is hoped that this work will provide a useful contribution to the ongoing SmartPlank research.

2.1 SmartPlank

The SmartPlank system consists of a small battery powered printed circuit board (PCB), which is connected to two thin foil strain gauges. The strain gauges are glued onto an aluminium plate (referred to as the strain gauge plate attachment). This plate is then screwed into a timber beam. An idealisation of the system is shown in Figure 2.1. The PCB is programmed to periodically read the strain measurements, and transmits the data over a wireless network to a computer on site, which records the data and can send it over the internet to the CUED.

Figure 2.1: Idealisation of SmartPlank system

The plate attachment (show in Figure 2.2) was developed in order to avoid using inflammable epoxy adhesives on site, which would otherwise be required to fix a strain gauge directly to timber. It is made of aluminium alloy 6028. The two plates for the two strain gauges are attached to the top and bottom of the beam, to read tension and compression results.

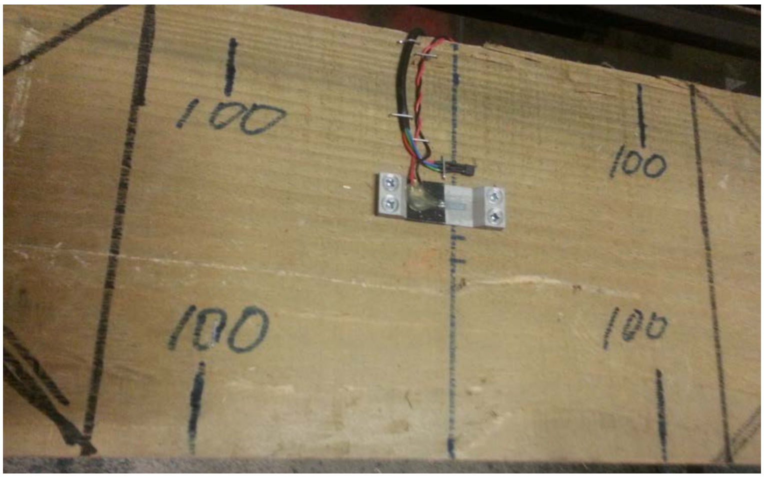

Figure 2.2: The plate attachment screwed onto a timber beam on site

This system is currently still in development, the idea being that when it is ready, many hundreds of strain gauges can be installed on many timbers at an underground construction site. This would allow an unparalleled insight in to the real performance of timber.

2.2 Aims

The aim of this project is contribute to an improvement in understanding of the real loads applied to timbers in underground construction, as part of the SmartPlank project. It is hoped that a greater understanding could be used to improve designs in the future.

The specific areas which this project aims to do this are:

1. investigation of literature pertaining to design methods and monitoring of timbers
2. investigation of data already collected by SmartPlank
3. develop a greater understanding of this data
4. investigation and improvement in the performance of the method of measuring strain currently used by SmartPlank

3 Literature Review

3.1 Historical Design of London Underground Timber Structures

Timber used in underground construction in the UK has primarily been used in London Clay soils, in London Underground (LU) projects. Hence, the majority of historical examples come from the LU, which has heavily influenced the design of underground timber structures. This review will report mainly on these historical designs, based on *Traditional Timbering in Soft Ground Tunnelling, A Historical Review* (Mackenzie 2014).

3.1.1 Reasons for Support Use

The use of 'traditional timbering' ground supports arose due to two important characteristics of London Clay. Firstly, London Clay contains many seams of discontinuities which are known as 'greasybacks', which were formed during tectonic movements between 5 and 35 million years ago, when the clay was deposited below a warm and shallow sea. These greasybacks can be inclined at up to 45° to the horizontal, and are coated in a paste which is similar in resemblance to heavy engine grease. Therefore, tunnelling may leave exposed a wedge of clay, held by two intersecting discontinuities; which can slide out of the face and into the tunnel. Thus as the soil is excavated, support is required to prevent: injury to workers and halting of tunnel progression.

Secondly, when exposed to air London Clay quite rapidly dries out. If this occurs, the soil loses its cohesiveness and degrades into a mass of loosely assembled small cubes which will fall off the tunnel face unless drying out is prevented, or the material is restrained. For this main reason grouting is pumped between the clay face and the timber supports (this is still done today, and will be discussed later in section 4).

The primary reasons for using timber are: it is a lightweight material, it can be easily cut and sawn into shape to suit local requirements, and is available in a wide range of dimensions. In addition, timber has excellent load bearing capabilities.

3.1.2 Structural Design

London Clay being a fairly consistent material, and the London Underground having had standard tunnel diameters, led miners and pit bosses to believe that no calculations were being made, since designs were often repeated. However, design drawings were only produced by engineers, and in all cases the drawings had to be approved by the Resident Engineer, with input from the General Foreman and/or Agent. These men had unparalleled design experience. The designs (always in the form of drawings) were passed down from Senior Engineers, who amassed a library of completed successful designs. Often this meant that engineers did not repeat calculations when using referenced successful designs (perhaps unacceptable these days). Hence, there is little evidence of a consistent timbering design philosophy within the tunnelling industry. However, there is one documented example of design guidelines, the “Mowlem Bible”.

3.1.3 The "Mowlem Bible"

During the 1960's, John Mowlem & Company - the oldest construction company in the business, accredited with building the majority of the tunnelled sections of the London Underground network - was working on the Victoria Line. Due to the scale of the project, a large volume of timbering design drawings, known as the "Mowlem Bible", was produced to aid young design engineers. These drawings had no calculations, but each drawing (at scale 1:24) was detailed enough for the miners to construct the tunnels. The young engineers clearly needed a basis for which to carry out calculations for their new designs. Therefore, the Senior Engineers developed a set of guidelines to be used. These guidelines are summarised in a typical design diagram, shown in Figure 3.1. Some of these guidelines are quoted here:

1. 'The principal purpose of headboards is to protect face workers from falls of blocks of clay from the roof. Headboards should, therefore, be capable of carrying 6 feet of clay.' This is shown in Figure 3.1 by the segment labelled 'R'.
2. 'The purpose of the combination of face-legs, poling boards... and Military Trestling is to keep the whole face under control. The timbering for each stage of excavation, working down the face, frame by frame, should be capable of supporting a block of clay (a “greasyback wedge”) sliding frictionlessly out of the face...' This is shown in Figure 3.1 by the segments ('A' to 'E') at the face of the tunnel.
3. 'Short duration horseheads [timber beams carrying vertical loads], generally, should be designed to carry at least 25% of the soils overburden. Longer duration horseheads, including those in stations, and in concourses between parallel stations, should be designed to carry at least 40% of the soils overburden.' Although it seems that this guideline was largely not used.
4. '“Pre-loading” is a vital aspect of timbering philosophy and practice, the maxim being: “Keep the ground under control at all times. Never let it move. Impose yourself on the ground before it can impose itself on you”.'

It is clear that the primary design focal points are greasybacks, and preloading. The design engineers used the discontinuity lines in Figure 3.1 for design to ensure the waling beams and horseheads could cope with greasybacks. These discontinuities are designed to be at 45° (worst case scenario). As discussed in guideline 4, preloading is carried out on all timbers. This is to ensure that the timbers were 'proof stressed' to stresses greater than (perhaps significantly) the stresses they experienced in service. It is considered that this practice is most likely what has caused the hundreds of years of success of these designs, as it ensures that no weak timbers are used. Guideline 3 is thought to have come from advice given by academics at Imperial College, or Soil Mechanics Ltd., but it is unclear how closely this was followed; it is assumed that the greasybacks dominated design methodology.

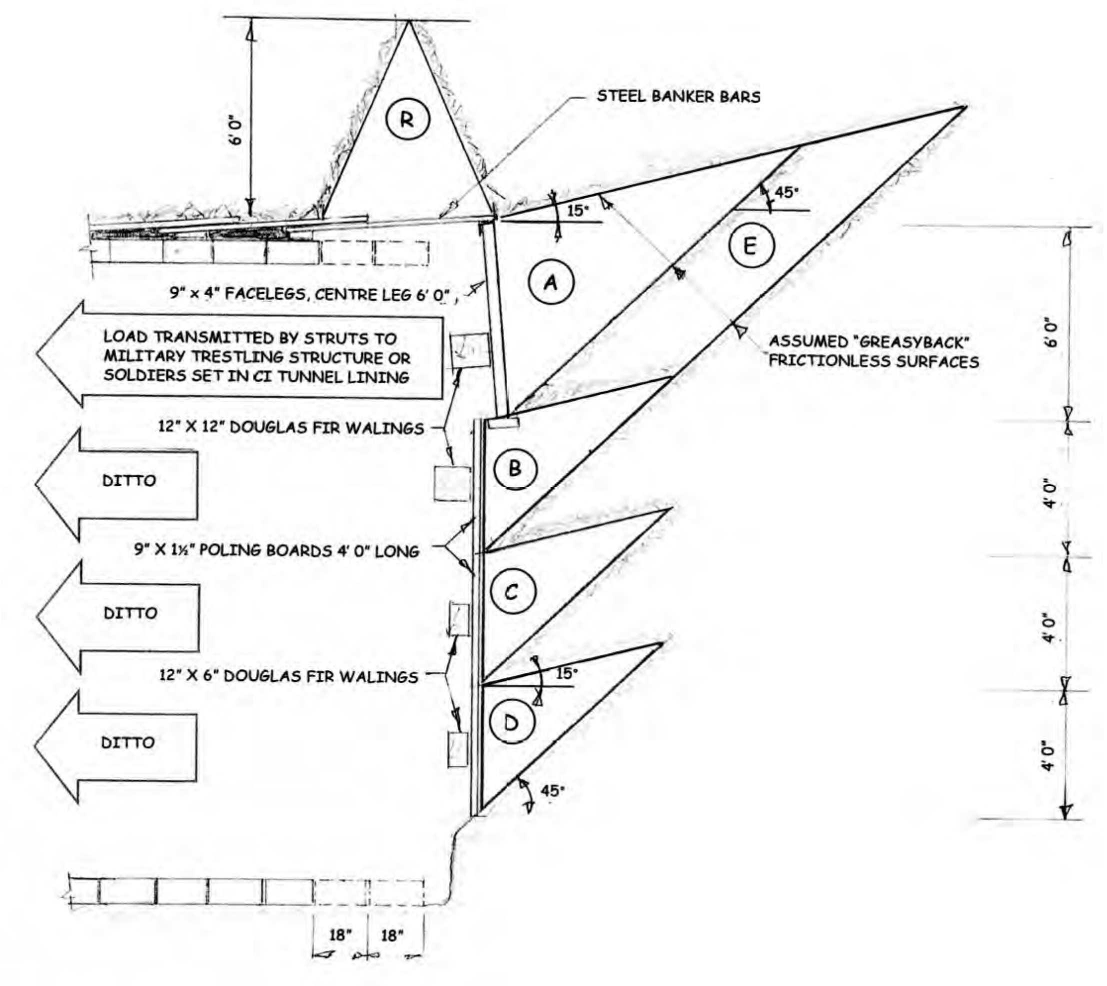

Figure 3.1: Timbering design check, along a section of the Victoria Line, circa 1964 (Mackenzie 2014)

3.2 Timber Roof Supports in the Mining Industry

The focus of this project is with timber as a temporary structural material, specifically in underground construction. This review will consider the temporary timber structures used in the mining industry, which is a more mature industry compared with underground construction for transport, for example. The mining industry mainly uses timber as props (columns, or pillars) to support rocky tunnel roofs.

3.2.1 Types of roof Support

Timber columns are used in mines to prevent collapse of the rock above. The current design methodology is to estimate the weight of the rock above, according to the 'fall-out height', and to allow an adequate number of supports for the given area (Ryder & Jager 1995). This 'fall-out height' is estimated according to previous observations, using the engineer's judgement.

There are 4 types of timber support, named according to their design behaviour: non-yield, yield, crush, and barrier pillars. The methods of design are mainly empirical, with each mine developing its own pillar design methods based largely on experience. The type of pillar most relevant to this project is the 'non-yield' pillar, which is primarily used for relatively shallow excavations.

3.2.2 Non-Yield Pillars

The main consideration for the design of non-yield pillars is to ensure that the strength of the pillars exceeds the maximum average pillar stress, at all times. The pillars are intended to remain intact and elastic throughout the life of the mine. Interestingly, the most important design tool used does not consider the material properties of the timber, but only its dimensions. The strength design equation is a theoretical equation modified empirically and is

$$\sigma_s = Kh^{\alpha}w^{\beta} \qquad (1)$$

where σ_s is the pillar strength; K is the strength of $1m^3$ of the rock; h is the pillar height; w is pillar width; and α and β are empirically derived constants. Therefore, the strength of the pillar is determined by the ratio (w/h), for a particular rock type. Figure 3.2 shows the stress-strain relationships for varying (w/h).

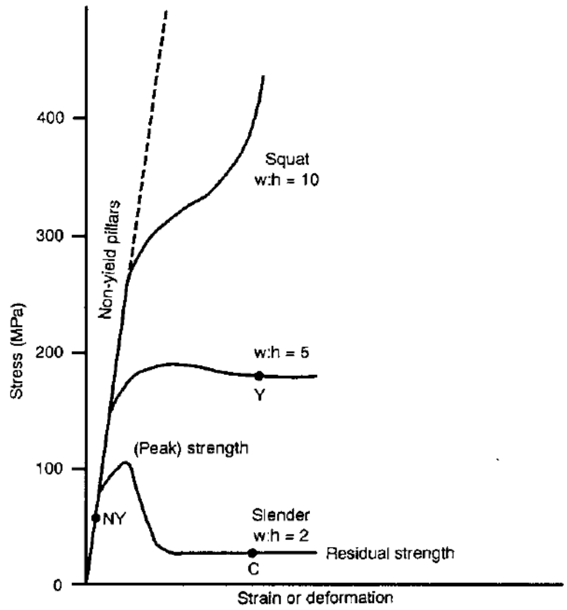

Figure 3.2: Typical stress-strain behaviour of hard rock pillars of different (w/h) ratios. Operating points are: NY = non-yield and barrier; C = crush; Y = yield. (Ryder & Jager 1995)

From Figure 3.2 it can be seen that the non-yield pillars (NY) are designed not to reach their peak strength. In the South African mining industry, a factor of safety of 1.6 is used as standard, however different values are recommended according to different research.

3.2.3 Recent Testing and Monitoring Developments

Recent advances have been made in quantifying failures of timber pillars used in mining (Daehnke et al. 2000). The failure mechanisms of the pillars depends on the angle of loading (which may be oblique due to improper installation, or irregularities in the rock surface). Therefore a test rig is used to vary the angle and rate of loading. A schematic of the test rig imposed load angles is shown in Figure 3.3.

A laboratory test rig can be used to investigate other factors which affect the failure of the timbers, other than contact and loading rate, namely temperature and humidity; and environment (e.g. moisture content, fungal invasion etc.). It has been shown that these factors can have a significant effect on the failure of timber.

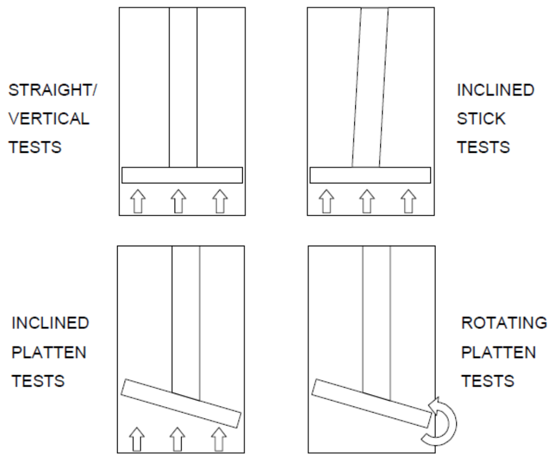

Figure 3.3: Illustration of test types using a lab test rig (Daehnke et al. 2000)

Tests and investigations like these have led to factors, or confidence intervals, within which the strength of an arrangement of pillars can be assumed to lie. It is possible for designers to use these confidence intervals dependent on the variables discussed here. However, many observations from underground sites have suggested that the actual strength of the support units is less than the strengths derived from laboratory tests. There is clear potential for SmartPlank to be used to monitor the in-situ behaviour of timbers used in mining.

3.3 Tottenham Court Road Design Review

London Underground's Tottenham Court Road station (TCR), is being upgraded as part of the Crossrail project, which will result in a rise in the number of passengers interchanging between LU services and Crossrail services. As a part of this expansion, a new staircase (Stair 14) is required between the Central Line platforms, in order to reduce congestion (this is shown in Figure 3.4) . In August 2013 work began on temporary works, required to create space and lifting facilities for the main works, about 20m below Oxford Street. The temporary works consists of reinforced concrete, steel columns bolted into the concrete, which support steel beams, in turn supporting timber head trees, in turn supporting the ground above. The tunnel sides are lined with timber side trees. A schematic of the temporary works construction process is shown in Figure 3.5. Later, the permanent works are installed (steel and concrete), but timber is only used as a temporary works material. At the start of construction, SmartPlank was installed on a beam which will be discussed later, in section 4, known as SmartPlank no.52.

Figure 3.4: Map showing location of stair 14 (map from maps.google.co.uk)

Figure 3.5: Construction sequence for the beam with SmartPlank no.52 installed, at staircase 14 (note: only structure relevant to SmartPlank no.52 and the design of timbers is shown).

This review will report in detail on the design methods for the timber head trees at TCR. Particular consideration will be given to the design assumptions and methods for timber temporary works in staircase 14 (where SmartPlank has already been installed), using the design report *Conceptual Design Statement (CDS) for Central Line Stair 14 Temporary Works (Phase 1)* (Aslte et al. 2013).

3.3.1 Design Methodology

3.3.1.1 General Loading

The type of structure most relevant to this project are shown in Figure 3.6 (which is the detailed construction drawing for the schematic in Figure 3.5, showing the central line tunnels), labelled as the timber head tree. In order to calculate the load applied to these beams, it is assumed that the timber head trees carry 15% of the total overburden. This is because the timbers are supported by steel or concrete after a week or two of their initial installation. The timber side trees are assumed to carry a horizontal load of 50% of the vertical load (i.e. 7.5%). (Long term loads are calculated using ground arching theories, such as Terzaghi and Protodyakavnov, and using FE analysis. This is done to establish the long term loads carried by steel or concrete permanent structure.) If a timber beam is considered to carry a long-term load (e.g. if permanent supports will not be installed for several weeks), then the timber is considered to carry 40% of the overburden. The design life for short-term support elements (timber head trees and side trees) is up to 1 month. This is considered to be conservative since stiff concrete filled steel spiles have been installed to protect a mid-level sewer in Oxford Street (shown in Figure 3.6), which will limit the ground loads acting on the timber headings constructed below.

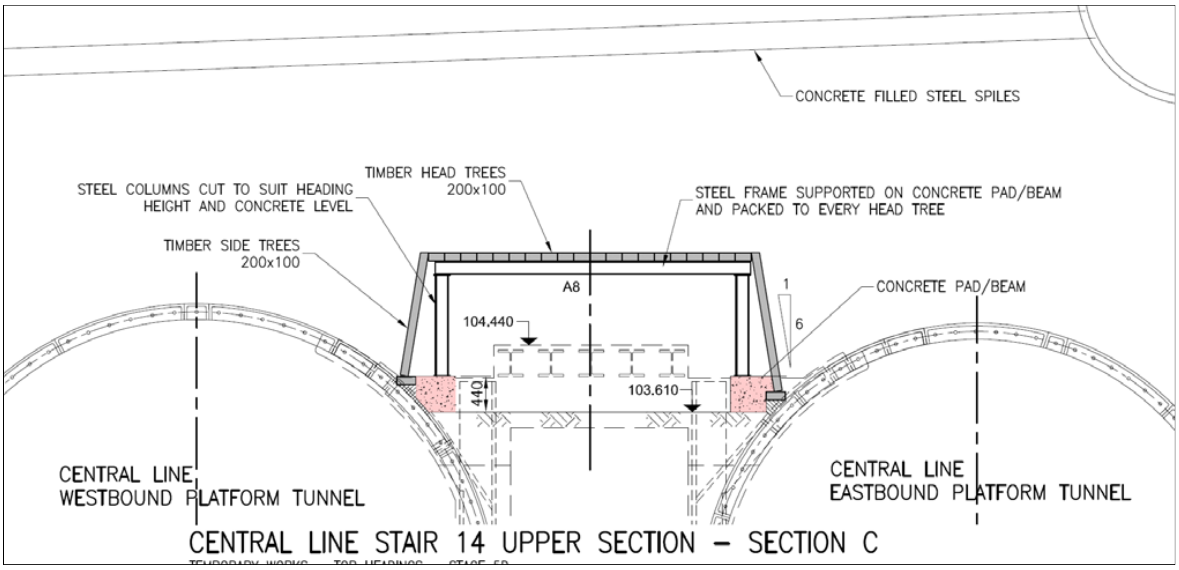

Figure 3.6: Detailed cross section of stair 14 (Aslte et al. 2013)

3.3.1.2 Structural Analysis

Once the loadings have been established, the timber elements are structurally analysed. This is done very simply. The loading, *w*, is assumed to be a uniformly distributed load (UDL), and the beams are considered to be simply supported, of length *l*, with no overhang (as shown in Figure 3.7), since this would have the conservative effect of reducing the maximum moment. This is the same for both the head trees and side trees. (Note: in the analysis of the head trees, the internal supports shown in Figure 3.5 are ignored.)

Figure 3.7: Simple model used in design of the timber elements

3.3.2 Detailed Design

The head trees and side trees at stair 14 were designed to take 15% of the overburden vertically, and 7.5% of the overburden horizontally. In this case, the overburden was calculated as 370.5kPa. The timbers were then designed to the ultimate limit state method prescribed in the Eurocode: BS EN 1995-1-1: 2004.

3.3.2.1 Material Properties

For C24 grade timber, a summary of the timber properties, safety factors, and design strengths used are shown in Table 3.1. The timbers used are 100mm x 200mm (height x width). The properties are taken from Table 1 BS EN 338: 2009. This table shows that the safety factor used in design, for the material properties of the timber, is equal to $(k_{mod}/\gamma_m) = 0.8/1.35 = 0.59$.

	Symbol	Meaning	Value
Properties	$f_{m,k,bending}$	Characteristic strength in bending	24 MPa
	$f_{c,0,k}$	Characteristic strength in compression	21 MPa
	ρ	Density	420 kg/m^3
Safety factors	k_{mod}	A safety factor which takes into account duration of load and moisture content	0.8
	γ_m	Material safety factor	1.35
Design Parameters	$f_{m,d}$	Design bending strength, equal to: $f_{m,k,bending}(k_{mod}/\gamma_m)$	14.77 MPa
	$f_{c,90,d}$	Design compressive strength, equal to: $f_{c,0,k}(k_{mod}/\gamma_m)$	12.92 MPa

Table 3.1: Summary of the material properties and safety factors used to design the timber head trees and side trees

3.3.2.2 Method

The design method for the head trees is as follows:

- The UDL, w, is calculated, from the vertical component of the overburden, and the timber self weight
- Axial load is calculated, from the horizontal component of the overburden
- These loads are multiplied by a dead load safety factor of 1.35
- Thus the maximum bending moment in the beam is given by $M_{mid}=1.35\,\frac{wl^2}{8}$ (for a simply supported beam)
- The design bending stress is calculated as: $\sigma_{m,d}=k_m\,\frac{M_{mid}y}{I}$, where k_m is a moment distribution factor, specified as 0.7 by the Eurocode, for ultimate limit state strength
- The design compressive stress is calculated as: $\sigma_{c,0,d}=1.35\,\frac{\text{Axial load}}{\text{Cross sectional Area}}$
- The overall strength of the beam is then checked with the equation:

  $$\frac{\sigma_{m,d}}{f_{m,d}}+\frac{\sigma_{c,0,d}}{k_{c,y}f_{c,0,d}}\leq 1 \text{ (=0.62 for the head trees at stair 14)}$$

  where $k_{c,y}$ is a safety factor combining material properties, dimensions, and empirically derived constants. This means that the compressive stress reduces the capacity of the beam, but only slightly (for the head trees at stair 14, $\frac{\sigma_{c,0,d}}{k_{c,y}f_{c,0,d}}=0.06$).

3.3.3 Monitoring of Timber Structures

Deflection of the timbers is segregated into a traffic light system. These are the expected deflections for three cases, which correspond to different loading:

- Green - unfactored stresses, essentially the conservative expected values (since they include the material safety factors), at 15% of the overburden
- Amber - ultimate limit state stresses, at 23% of the overburden
- Red - uses the ultimate limit state overburden multiplied by the material factor (1.3)

The method of calculating the deflections takes into account both bending deflection, and shear deflection. This requires values of the Young's Modulus (E) and Shear Modulus (G). They are taken from Table 1 BS EN 338: 2009. The values are: E=11GPa, and G=0.69GPa. These deflections are monitored daily using total stations, to ensure that the central deflections do not exceed the green trigger level.

3.3.4 Comparison with Historical London Underground Design

The design methods discussed here are quite different to those described in section 3.1. In exactly the same soil type, the historical design method essentially assumed that the timbers would carry a maximum height of 6m of clay (due to 'greasybacks'), whereas the modern design method assumes that the timbers will carry 15% (to 40%) of the full overburden. This means that the loadings are close to being the same if the timbers are at a depth of roughly 40m, and anything deeper than 40m means that modern designs are more conservative than historical designs (assuming a 15% of the overburden design load), and in shallower tunnels, historical designs are more conservative. These design values will be compared with the actual measured field values later in this report (see section 5.5).

3.4 Summary

Research carried out by the mining industry is leading to advances in methods of timber pillar design. These advances are largely borne from laboratory investigations. Other than in relation to the mining industry, there is a lack of literature available regarding the performance of timbers used in underground construction. Therefore, there is clear scope for research into timber performance from direct field measurements.

The present design methodology employed by the mining industry mainly considers the dimensions of the timbers, rather than the material properties and characteristics of the timber. However, for non-yielding pillars, this design method has the same outcome of aiming to prevent yielding of the timber, as the design method used in the modern TCR design. It is possible to see how research from projects such as SmartPlank could be used to develop a general design method for timber in underground construction.

4 Investigation of SmartPlank Results

4.1 Tottenham Court Road Installation

Four SmartPlanks were installed at TCR, during the construction of Stair 14, three of which had erroneous results due to electronics issues. Therefore, this project will focus on one of the four, known as SmartPlank no.52, which is shown in relation to the tunnel excavation in Figure 4.1.

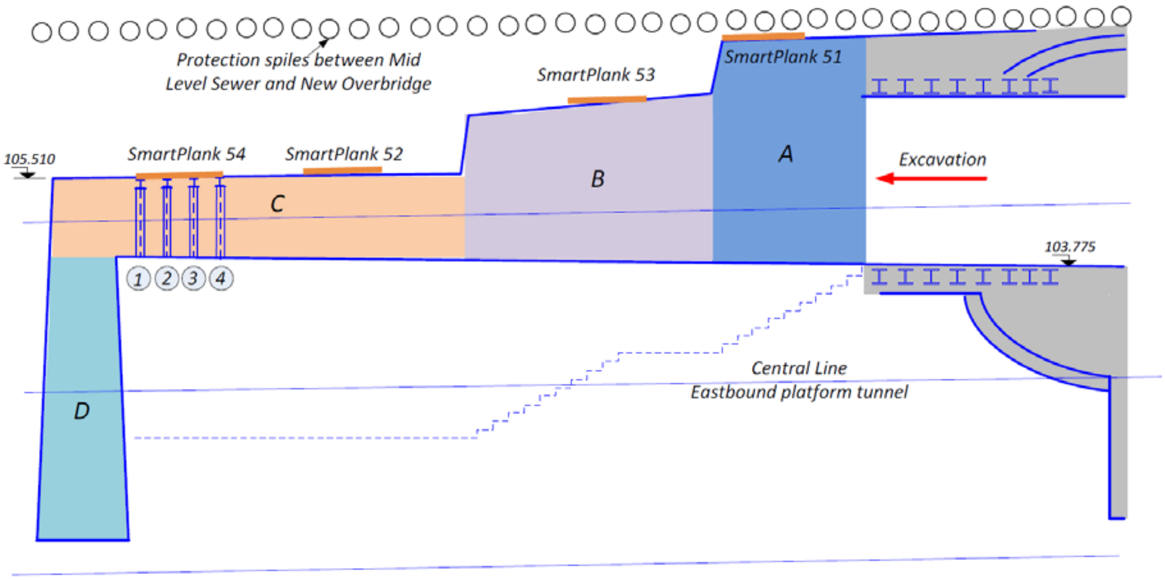

Figure 4.1: Longitudinal section of TCR stair 14 (Xu et al. 2015)

The construction sequence for the tunnel is as shown in Figure 3.5. From which, it can be seen that the timber beams end up resting on four steel beams. This is because only the outside supports were available at stage (1) shown in Figure 3.5, and the two interior supports were added one week later, at stage (3) in Figure 3.5. SmartPlank was switched on immediately upon installation. Therefore, the readings from SmartPlank correspond to two support cases, as shown in Figure 4.2. This construction sequence raises the important question: what strain should the installed strain gauges expect to measure?

Figure 4.2: Idealised section along the length of the tunnel at stair 14, showing the construction sequence for the beam which made up SmartPlank no.52

4.2 Results from Tottenham Court Road

The strain measured by SmartPlank no.52 at TCR is used to back-calculate the pressure applied to the beams, using a model developed by Xu et al. (2015). This allows a comparison to be made with the loadings used in design, as discussed in section 3.3. The model uses simple beam theory, and for the first week (case 1) directly uses the strain measured to calculate the load. In order to account for the change from case 1 to 2, after the first week (case 2), incremental changes in strain from the end of case 1, are used to calculate incremental changes in load, which are added to the load at the end of case 1. The back-calculated earth pressure for SmartPlank no.52 is shown in Figure 4.3. (The figure is dominated by case 2, since the interior supports were added only a week after 06/09/2013.)

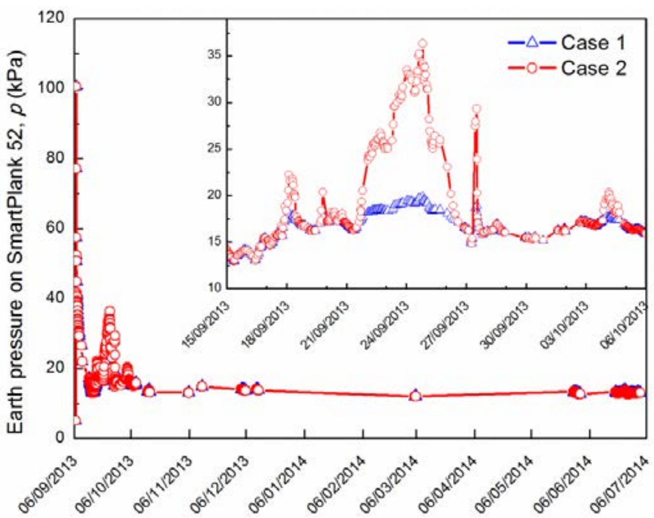

Figure 4.3: Back-calculated earth pressure for SmartPlank no.52, showing case 1 & 2 (Xu et al. 2015)

The results show that initial load was 100kPa, which is exactly the injection pressure of the grouting (as shown in Figure 3.5). After this, the load drops off to a residual load, which is the overburden. (The jump shown in case 2 prediction at 24/09/2013 is assumed to be due to installation of props during permanent works installation, which may have affected the timber.) These results are promising, however it was hypothesised that the model could be improved by computationally modelling the structure, to try and improve the beam theory based model, to account for effects such as support width.

It was decided to use a finite element modelling software, Strand7, to investigate the changes in strain in the timber beam, dependent on the number of supports and the width of the supports. Investigating the effect of the width of the supports allows results from Strand7 to be compared with beam theory predictions (when simply supported), which will validate the Strand7 predictions, and can then be compared with data already collected from TCR.

4.3 Finite Element Investigation

4.3.1 Overview of Strand7

Strand7 is a 3D visual environment which allows the user to create a model of the problem to be investigated, using a type of finite element solver specified by the user (i.e. linear or non-linear, static or dynamic, etc.). Material properties are assigned to each component of the model. The model consists of 'nodes', 'beams', 'plates' and 'bricks'. In this investigation, the timber is made of 'bricks', and the supports are made of 'plates' (which are assigned the relevant thicknesses of the steel web and flanges). Strand7 takes gravity into account.

4.3.2 Formulation of Elements

The shape functions used for the plates, and bricks, are the same functions used for plane stress, plane strain, and axisymmetric analysis. These shape functions are based on isoparametric mapping, which means that the initial geometry of an element, and its displacement components are based on the same mapping relationship between the element's natural coordinate domain and physical space. For the plate element, the coordinates (X) and displacements (u) of a point within the element can be expressed in the following forms

$$X(\xi_1,\xi_2) = \sum_{i=1}^{n} N_i(\xi_1,\xi_2)\, X^i \qquad (2)$$

$$u(\xi_1,\xi_2) = \sum_{i=1}^{n} N_i(\xi_1,\xi_2)\, d^i \qquad (3)$$

where

n = number of nodal points in the element

X^i = coordinate vector for node *i*

d^i = displacement vector for node *i*

ξ_1, ξ_2 = natural coordinates

$N_i(\xi_1, \xi_2)$ = shape function for node *i*

For brick elements, the coordinate and displacement equations are the same, except with three natural coordinates ξ_1, ξ_2, ξ_3.

4.4 Method

The model designed in Strand7 has a resolution of 20mm x 20mm. This means that the nodes which make up the corners of the plates and bricks, are arranged in a square shape of side length 20mm. For the plates, which make up the steel supports, these squares are 2D, but are assigned a thickness. For the bricks, which make up the timber beam, these squares are 3D. The consistency in node density between the plates and bricks ensures a uniformity in the mesh, which is important for modelling the contact between the steel supports and the timber beam.

In between the nodes of the supports and the timber, a 'point contact beam' is used to connect the nodes (which are 10mm vertically apart). Point contact beams provide stiffness only in compression, which is an accurate model of the real situation. The stiffness is dynamic, which means that as the load is increased by the solver, the stiffness of the point contact beam is adjusted to a more suitable value, depending on the situation of the state of the gap/contact. in order to model this function, a non-linear solver is required. The point contacts also simulate friction, however in the models used here it has been found that varying friction had no effect on the results. Figure 4.4 shows the point contact beams in relation the rest of the model.

Figure 4.4: Close up of the steel support - timber beam contact

The steel beams are restrained at the bottom of both ends, so are fixed in position, unable to move or rotate. The steel beams are 1000mm in length. A uniformly distributed load is applied to the top surface of the timber beam. Since the resolution of the model is 20mm (otherwise it takes too long to solve), the geometry of the situation is changed very slightly, compared with the real construction shown in Figure 4.2.

The results from Strand7 should be compared with beam theory in order to validate them. For this reason the support width is varied so that the simply supported case can be compared with a beam theory calculation. The width of the supports is initially 200mm, and is reduced in increments of 40mm down to 0mm (i.e. simply supported). The method of reducing the width is to remove the point contacts between the timber and the steel. A comparison of the Strand7 and beam theory models, for cases 1 and 2 are shown in Figure 4.5 and Figure 4.6.

Figure 4.5: Comparison of the beam theory and Strand7 models for case 1

Figure 4.6: Comparison of the beam theory and Strand7 models for case 2

The actual Strand7 model of the case 1 beam is shown in Figure 4.7, where the applied load can also be seen on the top surface of the timber beam. Note that all the squares that can be seen in Figure 4.7 are 20mm x 20mm, and that the case 2 model is identical apart from the extra internal supports.

Figure 4.7: Actual Strand7 model for case 1

4.4.1 Applied Load

This investigation was carried out over a variety of loads, so that a relationship could be found between load applied and strain measured (as a ratio of beam theory predictions) over a constant support width. This can then be used to create a prediction for the expected strain from the strain gauges at TCR, for when the supports are 200mm (full width).

4.4.2 Beam Theory Calculations

In order to calculate the moment distribution, and therefore the strain distribution in the beam, Macauley's method was adopted. This method employs the use of the Macauley function, which has the properties:

$$\{x-l\}^n = \begin{cases} 0, & x \leq l \\ (x-l)^n, & x > l \end{cases}$$

which makes the generation of the moment distribution, for example for between supports C and D (in Figure 4.8), easy to write down as

$$M(x) = R_A\{x-a\} + R_B\{x-(b+a)\} + R_C\{x-(c+b+a)\} - \frac{wx^2}{2} \tag{4}$$

but note that this equation is only valid when x is between the supports C and D. Differentiating equation (4) twice generates the displacement equation for between supports C and D. In order to find all of the reactions, the moment equation for when x is between support D and the end of the beam is twice differentiated, to find the displacement (δ) equation for the beam:

$$EI\delta = \frac{R_A}{6}\{x-l_1\}^3 + \frac{R_B}{6}\{x-l_2\}^3 + \frac{R_C}{6}\{x-l_3\}^3 + \frac{R_D}{6}\{x-l_4\}^3 - \frac{wx^{24}}{24} + C_1x + C_2 \tag{5}$$

where $l_1 = a;\ l_2 = a + b;\ l_3 = a + b + c; l_4 = a + b + c + b$; and C_1 , $C_2$are constants and EI is the stiffness of the beam. Applying the boundary condition of there being zero displacement at all of the supports to (5), and by observing vertical and moment equilibrium, generates 6 equations and 6 unknowns (R_A, R_B, R_C, R_D, C_1 and C_2). These 6 equations can be solved by creating a 6x6 matrix, and using the relationship $x=A^{-1}B$, in Matlab, for example.

Figure 4.8: Beam theory model for 4-support beam

Solving the 6x6 matrix, and using the geometries shown in Figure 4.5 and Figure 4.6 reveals the following relationships:

- $R_A = R_D$ = 810w for case 1, and
- $R_A = R_D$ = 306.3w, $R_B = R_C$ = 503.7w for case 2

These reactions are used to calculate the moment at the locations of interest in the beam using equation (4). The strain is then calculated using $\varepsilon = \frac{My}{EI}$, where y is the distance from the neutral axis to the extreme fibre (which is 50mm for this timber beam).

4.5 Results & Discussion

4.5.1 Case 1

The results for case 1 were encouraging. Figure 4.9 shows the Strand7 strain predictions, compared to beam theory. As one would expect, a wider support leads to a reduction in the strain in the beam, which can be seen in Figure 4.9, which also shows that the results for the top and bottom of the beam were identical in magnitude. This relationship is also true for the results at the centre of the beam.

Now, introducing a non-dimensionalised strain $\boldsymbol{\varepsilon}_{S7/BT} = \frac{\text{Strand 7 Results}}{\text{Beam Theory Prediction}}$, which can be plotted against either support width or load for further investigation. This relationship of $\boldsymbol{\varepsilon}_{S7/BT}$ with support width is shown in Figure 4.10 for the centre of the beam, and the location of the strain gauges at TCR. From this plot, it can be seen that the reduction in strain is fairly constant until the support width is reduced to around 80mm. When the support width is reduced to 0mm, and is essentially the ideal beam theory assumption, the strain predicted by Strand7 agrees with beam theory. Therefore we can confidently use Strand7 predictions for case 1, to compare with measured data from TCR. Figure 4.10 shows that there is a relationship between the location in the beam and the value of $\boldsymbol{\varepsilon}_{S7/BT}$, which appears to get closer to unity at the location in the beam where the strain value is largest.

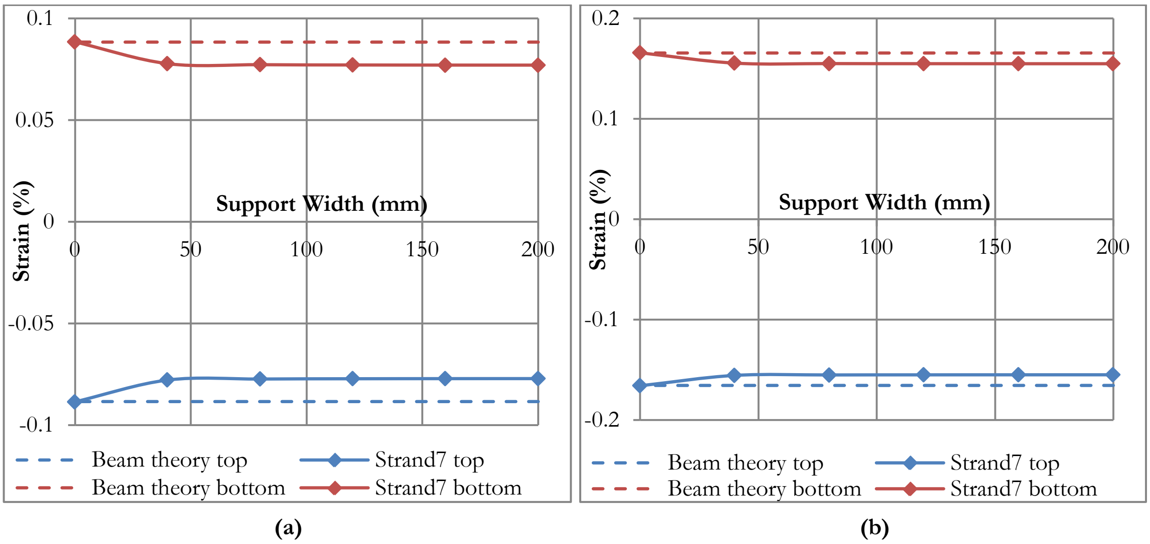

Figure 4.9: Comparison of strain predicted by Strand7, with beam theory, for the top and bottom of the beam.
(a): Location of the strain gauges at TCR
(b): Centre of the beam

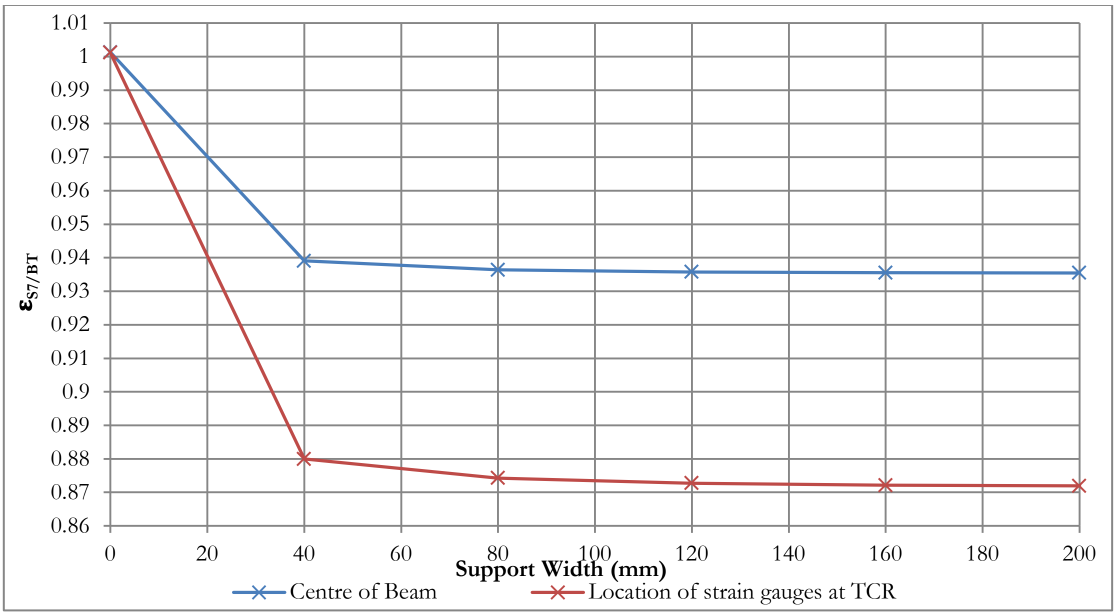

Figure 4.10: $\boldsymbol{\varepsilon}_{S7/BT}$ versus support width for case 1

Given that the results for case 1 have been validated, a relationship is now required which shows the Strand7 strain predictions for varying load, for when the supports are at full 200mm width. This relationship will be used to compare the Strand7 predictions with the data from the strain gauges at TCR.

Plotting $\boldsymbol{\varepsilon}_{S7/BT}$ against a varying load (as shown in Figure 4.11(a)), reveals that when the load is greater than around 60kPa, the value of $\boldsymbol{\varepsilon}_{S7/BT}$ is roughly constant, with an average value of 0.87 (to 2 significant figures). Below around 60kPa, the smaller the load becomes, the more variable the value of $\boldsymbol{\varepsilon}_{S7/BT}$. This is possibly to do with the self weight becoming more dominant, or to do with the solver. A zoomed out plot of $\boldsymbol{\varepsilon}_{S7/BT}$ versus applied load is shown in Figure 4.11(b), which shows how $\boldsymbol{\varepsilon}_{S7/BT}$ is essentially constant.

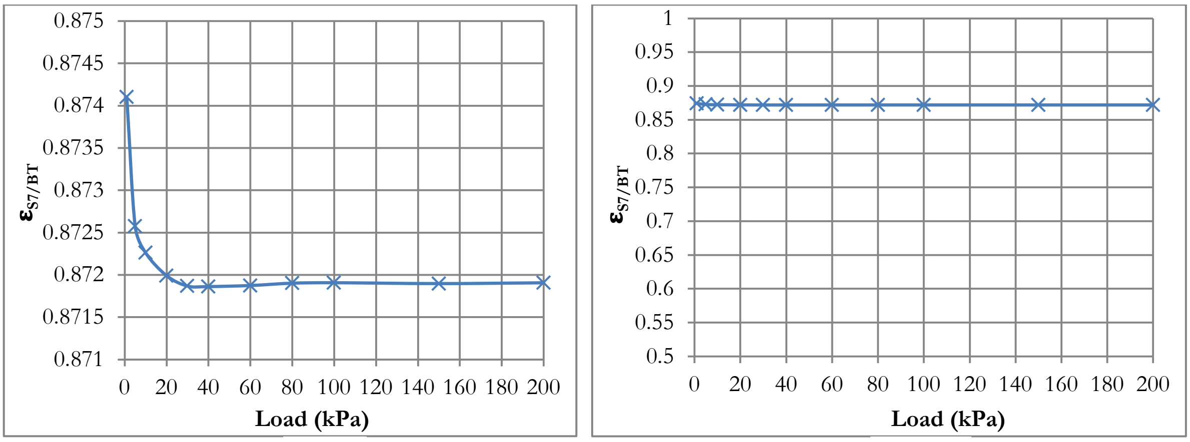

(a) **(b)**

Figure 4.11: $\boldsymbol{\varepsilon}_{S7/BT}$ versus load applied, for the case 1 beam at full support width. Scale is varied to appreciate the small variation in $\boldsymbol{\varepsilon}_{S7/BT}$. This is for the location of the strain gauges at TCR.

To summarise these results, it was found that:

- supports being wider than 0mm reduces the strain in the beam, compared to beam theory predictions;
- when the support width is reduced to 0mm, the results agree with beam theory;
- although it is not possible to be certain that the actual supports at TCR provide 200mm of support, it has been shown that when the support width is greater than around 80mm, there is little variation in $\boldsymbol{\varepsilon}_{S7/BT}$, so this does not matter;
- and that with a varying load, the value of $\boldsymbol{\varepsilon}_{S7/BT}$ is essentially constant.

Thus, to compare with data from TCR, a value of $\boldsymbol{\varepsilon}_{S7/BT} = 0.87$ will be taken.

4.5.2 Case 2

Results of the Strand7 strain predictions compared with beam theory are shown in Figure 4.12. These results clearly follow a different relationship to the results from case 1. (Note that in terms of the model and solver used in Strand7, both case 1 and case 2 are entirely identical - other than the addition of two interior supports for case 2.)

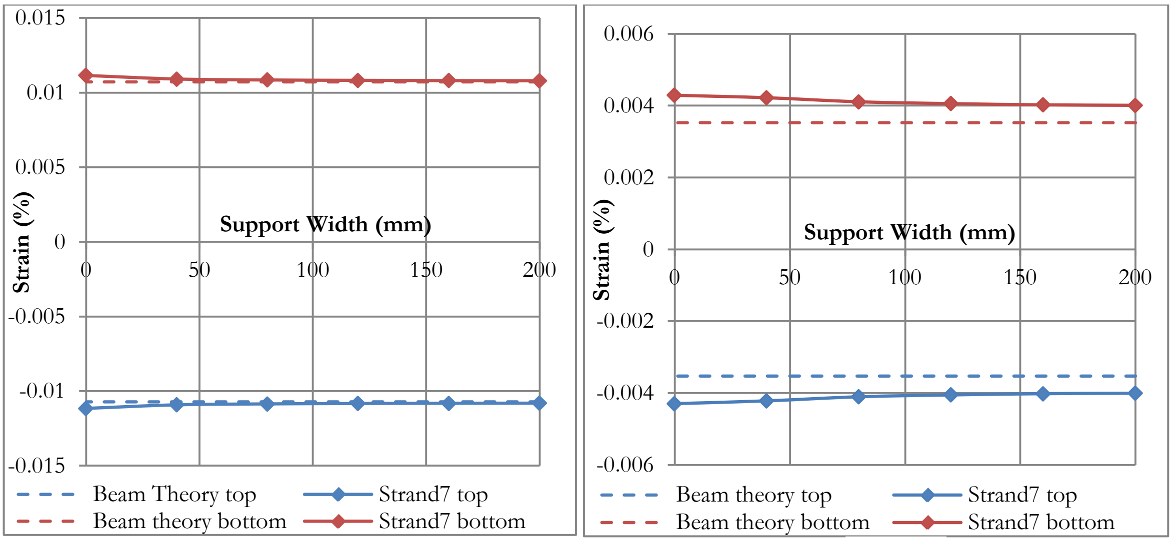

(a) **(b)**

Figure 4.12: Comparison of strain predicted by Strand7, with beam theory, for the top and bottom of the beam.
(a): Location of the strain gauges at TCR
(b): Centre of the beam

A closer inspection of the relationship of $\boldsymbol{\varepsilon}_{S7/BT}$ with support width is shown in Figure 4.13.

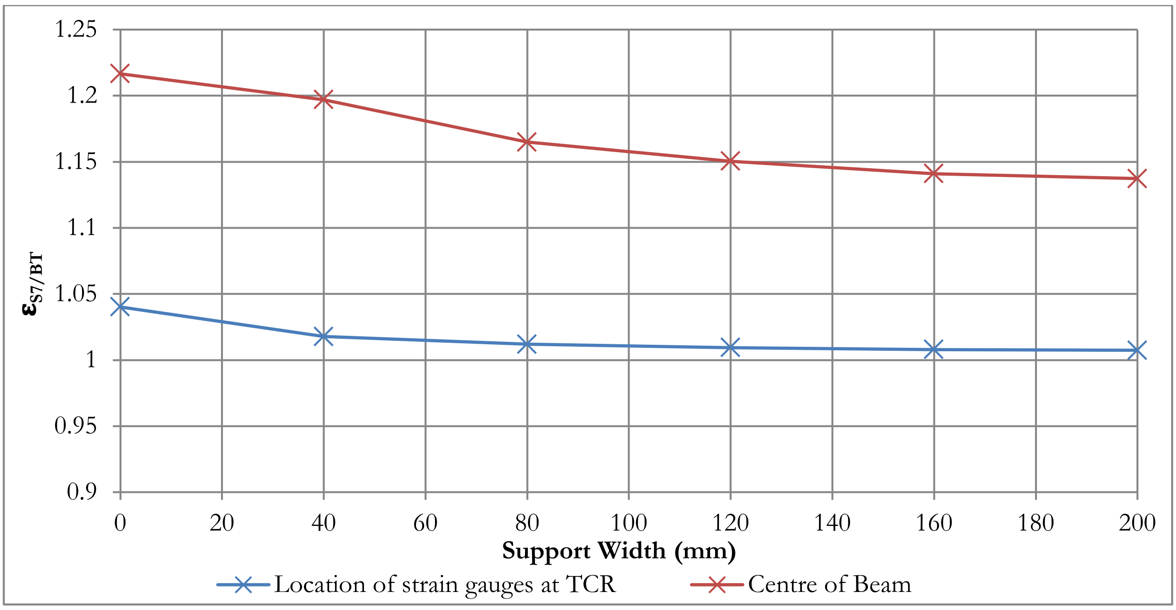

Figure 4.13: $\boldsymbol{\varepsilon}_{S7/BT}$ versus support width for case 2

From Figure 4.13 it can be seen that the value of $\boldsymbol{\varepsilon}_{S7/BT}$ is not as constant as it is for case 1. In addition, $\boldsymbol{\varepsilon}_{S7/BT}$ is greater than unity, meaning that Strand7 is over-predicting the strain (compared to beam theory). It is quite unclear why this might be happening. An investigation was carried out to confirm that there were no variables within the model which may be causing unusual results.

The friction modelled by the point contacts (as discussed in section 4.4) was varied, to see if this had an effect (even though it shouldn't). Also, the solver was varied. Ordinarily the model runs a linear geometry through a non-linear solver, so a check was made to ensure the a non-linear geometry did not produce different results (even though it shouldn't). It was found that these variations had no effect. One possibility is that the greater number of supports has reduced the accuracy of the model. The trend of increasing strain with reduction in support width is still seen. A closer inspection of the location of the strain gauges at TCR will now be made.

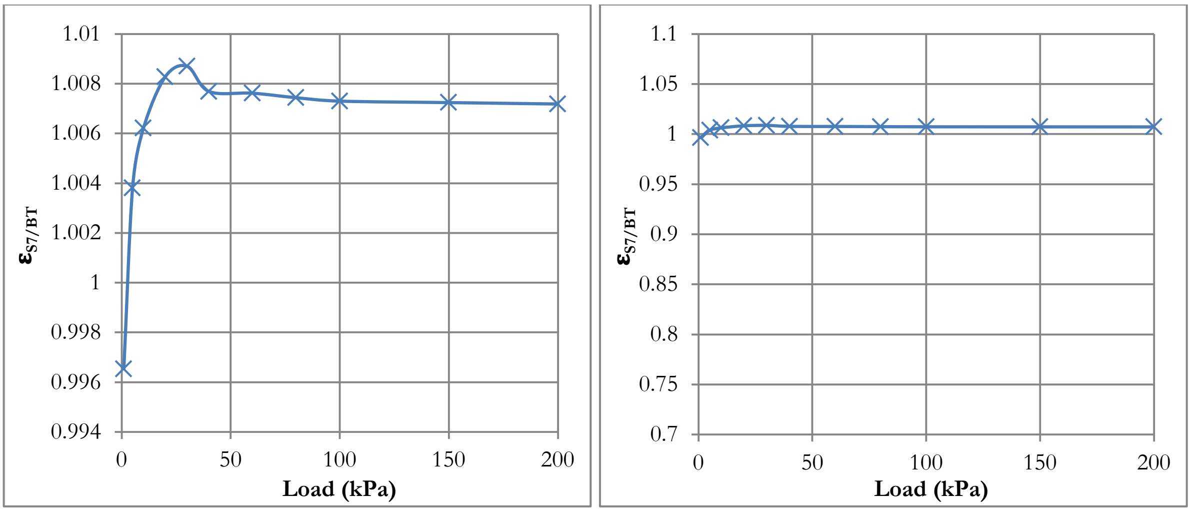

Figure 4.14: $\boldsymbol{\varepsilon}_{S7/BT}$ versus load applied, for the case 2 beam at full support width. Scale is varied to appreciate the small variation in $\boldsymbol{\varepsilon}_{S7/BT}$. This is for the location of the strain gauges at TCR.

Figure 4.14 shows the variation of $\boldsymbol{\varepsilon}_{S7/BT}$ with applied load. As with case 1, it can be seen that at lower loads $\boldsymbol{\varepsilon}_{S7/BT}$ changes in behaviour, however, at loads greater than around 50kPa, $\boldsymbol{\varepsilon}_{S7/BT}$ is fairly constant. Although it is less intuitive to understand these results compared with case 1, since $\boldsymbol{\varepsilon}_{S7/BT}$ is close to unity for the location of the strain gauges at TCR, $\boldsymbol{\varepsilon}_{S7/BT}$ will be taken to be unity for comparison with TCR data.

4.6 Comparison with TCR Data

The values of $\boldsymbol{\varepsilon}_{S7/BT}$ found for cases 1 and 2 in the previous sections are used to estimate the back-calculated earth pressure, from the strain measured at SmartPlank no. 52 at TCR (shown in Figure 4.15), using the beam theory model from (Xu et al. 2015), who predicted the maximum strain to be 100kPa. The values of $\boldsymbol{\varepsilon}_{S7/BT}$ developed in this project shows that this maximum strain is more likely to be around 115kPa. This coincides with the time at which grouting is injected between the timbers and the clay, which occurs at exactly 100kPa. The purpose of the grouting is as described in section 3.1. Following installation, the back-calculated earth pressure drops to just below 20kPa.

This is a promising result, since the grouting was injected at 100kPa, and the load predicted at this time is roughly 115kPa, which then drops by around 100kPa to just below 20kPa, suggests that the measured strain is picking up the pressure of the grouting plus the overburden at the start, and then dropping to the residual overburden pressure. It appears that this was not being picked up before.

Therefore, the vertical design load of 15% of 370.5kPa, multiplied by a safety factor of 1.35 (equal to 70kPa), as discussed in section 3.3, is very conservative in the long term. Grouting is not currently considered in the design of the beams. Perhaps grouting should be given a consideration during design. This is identified as an area for further research.

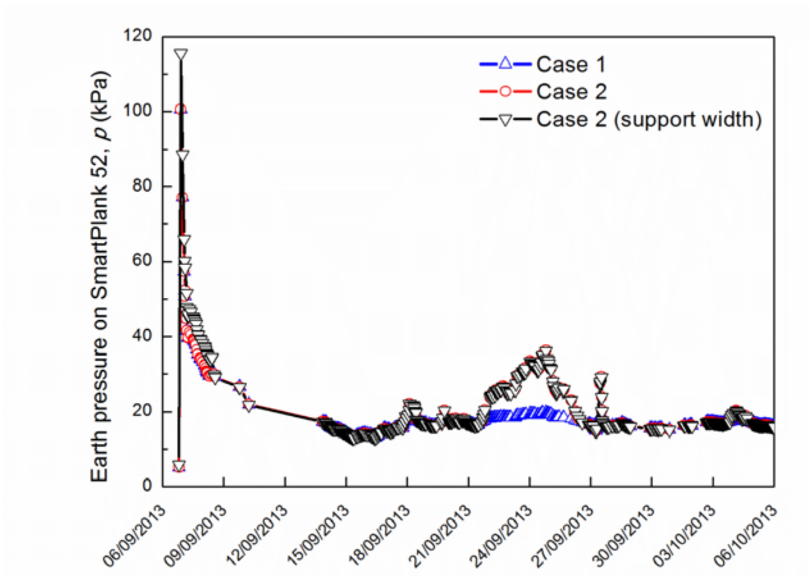

Figure 4.15: Estimated variation of earth pressure on SmartPlank 52.
Case 1, Case 2 : predictions for simply supported beam
Case 2 (support width): predictions with 200mm wide supports

5 Strain Gauge Measurement

5.1 Previous Design

5.1.1 Design Process

The concept of using a ductile metal plate to attach a strain gauge to timber (as described in section 2.1) was developed by *David Cheuk*, a previous MEng student (Cheuk 2012). The primary reason for this was due to the intended location of installation: at TCR, the contractor insisted that epoxy was not used during the deployment. Epoxy is required to attach a foil aluminium strain gauge to a material of interest. Using epoxy on site required a COSHH assessment, which was deemed too time and cost intensive. Therefore, the strain gauge must be glued using the epoxy to a device prior to deployment on site. This device can then be attached to a beam on site using, for example, screws instead of epoxy, which is a great deal more practical.

The design created is shown below in Figure 5.1. This plate is made of aluminium alloy 6028, which was chosen because it was readily available; did not have a very high stiffness (so should not reinforce the beam below); has a high yield stress (so should deform uniformly with strain); and is easy to machine. The region where the strain gauge is glued is intentionally very thin, so as to not cause any local reinforcement to the timber beam (since it is inferred that the strain which the strain gauge measures - in the aluminium plate - is actually the strain in the beam structure below). With regards to the shape of the plate, it is unclear what methods were employed to derive its overall dimensions, other than that "the sides of the plate were designed to be thick enough to ensure a good local transfer from the plank to the gauge" (Cheuk 2012). It appears no consideration was given to behaviour of the plate under compressive strain (i.e. buckling behaviour).

Figure 5.1: Original design of strain gauge attachment plate

5.1.2 Cheuk's Analysis of Design Performance

Experiments carried out by Cheuk showed that the design produced quite a good linear relationship when tested on timber, although the gradient produced was lower than expected (compared to beam theory, and an epoxy attached strain gauge). Figure 5.2 shows the results of a hanging weight experiment carried out by Cheuk.

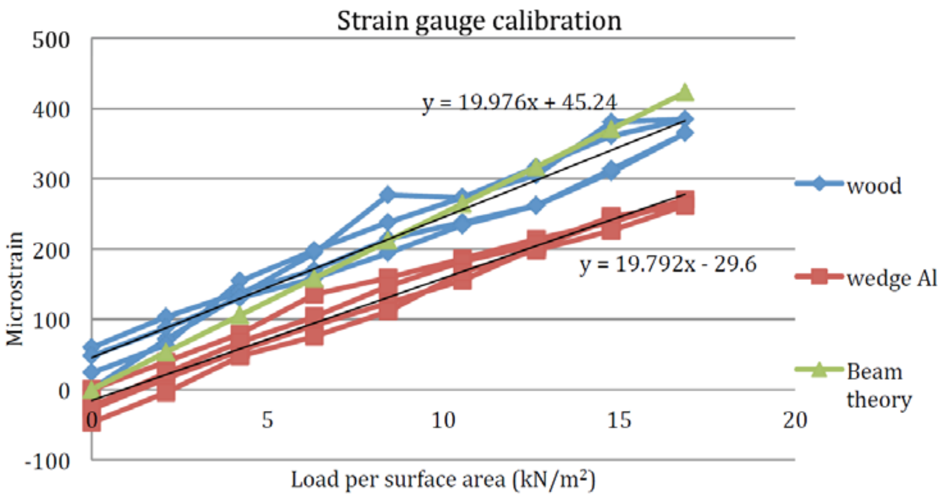

Figure 5.2: Comparison of readings from strain gauges attached by the plate, and by epoxy, onto wood, vs. beam theory predictions (Cheuk 2012)

For the purpose of deployment at TCR, these results were acceptable. They show that the plate attachment (shown as 'wedge Al'), had a reasonable linearity, although it had a gradient slightly less than beam theory. However, it does seem that there could be benefit in verifying these results, which would allow greater confidence in the results discussed in section 4.6. It was therefore decided to examine the performance of the plate attachment, using a 4-point bending test rig.

5.2 Theory and Design of Experiments

5.2.1 4-Point Bending

To assess the performance of the strain gauge plate attachments, a simple 4-point bending experiment is used. A 4-point bending test rig creates a region of constant strain in the beam between the two internal supports. Figure 5.3 below shows the idealisation of a 4-point bending experiment.

Figure 5.3: Schematic of the 4-point bending experiment set-up (not to scale)

The theoretical value of the central strain can be derived using simple beam theory as follows: the moment induced in the centre of the beam due to downwards displacement of the supports (as shown below in Figure 5.4) is

$$M = Fa \tag{6}$$

Where F is the force applied by the downward displacement of the supports, and *a* is as shown in Figure 5.3.

Figure 5.4: Diagram considering the central section of the beam (not to scale)

Now, because there is zero rotation at the centre of the beam, half of the centre of the beam can be modelled as of the form shown in Figure 5.5, using symmetry:

Figure 5.5: Model used to analyse the central deflection of the beam, using the standard structures databook case

The central deflection of the beam, δ, is therefore given as:

$$\delta = \frac{Ml^2}{2EI} = \frac{aFl^2}{EI} \tag{7}$$

Which is the standard CUED structures databook case. Now, the strain developed is

$$\varepsilon = \frac{My_{max}}{EI} = \frac{aFh}{2EI} \tag{8}$$

Rearranging equation (7) and substituting into (8), the equation for the central strain is derived:

$$\varepsilon = \delta \frac{h}{l^2} \tag{9}$$

Thus only the height and central length of the beam are required to estimate the strain in the beam, given the central displacement (as measured by a dial gauge).

5.2.2 Assumptions

- The beam is a linear elastic material, of zero self-weight, and undeflected (straight) when there is no applied moment.
- The stiffness of the strain gauge plate has no effect on the stiffness of the beam, such that the beam is not strengthened at the point where the plate is fixed, and therefore does not influence the strain in the beam.
- The extra height of the plate means that the strain gauge, will be measuring the strain at a point slightly above the surface of the beam. It is assumed that this extra height is negligible.

5.3 Apparatus & Experimental Techniques

5.3.1 Equipment

4-Point Bending Rig

The rig works as shown in Figure 5.3. In order to induce the displacements, a gear is turned by hand, which very slightly displaces the end supports downwards.

Beams

Two types of beams were used for experiments: steel and timber. The steel beam was standard steel and had dimensions 25mm x 50mm x 1320mm. The timber beam had unknown properties (this is discussed later) and had dimensions 45mm x 45mm x 1320mm.

Dial Gauge

The method of measuring the central deflection of the beam was a 0.01mm/div micrometer. The beam was deflected in increments of 20 divisions, which is 0.2mm. Therefore, the accuracy of the dial gauge was 0.2 ± 0.005mm which is an error of 2.5%.

Torque Wrench

The torque wrench is manufactured by Gedore (model no. 4549-00 TorcoFix K) and has a tolerance which is certified to ±3%. The minimum torque used was 4Nm therefore the maximum error was ±0.12Nm, which is not very large.

PCB & Laptop

The PCB has 4 input channels, each of which forms one leg of a Wheatstone bridge, and is connected to a an analogue to digital converter (ADC). The PCB is powered by 2 AA batteries. The PCB is wirelessly connected to the laptop, to transfer data packets (using Contiki-OS and Wireshark software). The data file is then analysed using a Matlab script which converts the raw data into plots of strain versus time.

Strain Gauges

The strain gauges used are 120Ω 5mm RS foil gauges, which are carefully epoxy glued onto the middle part of the plate attachment, by first sanding and cleaning (using acetone) the metal surface. The strain gauge is aligned to be in the exact middle of the plate, and parallel to the plate edges. Flexible wiring is then soldered onto the strain gauge electrical leads. A change in the length of the strain gauge causes a fractional change in the resistance of the gauge. The proportion of this change is called the gauge factor (GF), which is 2.1 for these strain gauges. To calculate the real strain, the output voltage is measured and using the GF it is converted into strain.

5.3.2 Experimental Design

The procedure of the experiment is:

- When testing on steel, the strain gauge plate attachment is bolted onto the centre of the beam, to a particular torque measured using the torque wrench. When testing on timber, the plate attachment is screwed into the beam as tightly as possible. In the centre of the beam is also a strain gauge directly glued to the surface of the beam. These two strain gauges are both connected to the PCB, which is wirelessly connected to the laptop.
- Using 'Wireshark' software the readings from the strain gauges are recorded into a .csv file.
- The end supports of the 4-point bending rig are displaced, such that the centre of the beam is displaced upwards from 0mm to 1mm, and back down to 0mm, in increments of 0.2mm. These increments are chosen to give a good range of readings from the strain gauges. In addition, this provides a factor of safety of 3 against failure of the steel beam, which means that repeated experiments should not affect the properties and performance of the steel beam.
- The beam theory prediction of the value of strain is estimated using the measured central displacement, combined with equation (9)
- The recorded measurements of strain are converted from a .csv file into plots of strain versus time (using Matlab), and then plotted against the beam theory predictions.
- If there were clearly erroneous results, for example if a strain gauge was not properly connected to the PCB, then the experiment was re-run.

This allows a comparison to be made of the strains: estimated using beam theory; measured with a strain gauge directly glued to the surface of the beam; and measured using the strain gauge plate attachment. If the beam theory estimation agrees well with the strain measured by the strain gauge which is glued to the beam, then the accuracy of the strain measured by the plate attachment can be established.

5.4 Performance of Previous Design

5.4.1 Tension Results

The performance of the original design was assessed using the 4-point bending test rig, on a steel beam. Figure 5.6 shows the results of testing of the original design, in tension experiments. The plot also shows that the strain gauge which was glued directly to the surface of the beam, produced results very close to beam theory predictions. This means that is it acceptable to consider the strain estimated using beam theory as being the actual strain in the surface of the beam.

It was quickly found that the amount of torque in the bolts affects the linearity of the readings. Bolts which were tightened by hand (to an unknown torque) resulted in poor, non-linear strain results, with a magnitude much lower than that of beam theory. By increasing the torque in the bolts to 2Nm (the limit of an M3 bolt), using a torque wrench, the results had a much greater linearity, and a magnitude close to beam theory predictions. This raised the question, that if the torque in the bolts were greater, would the linearity of the results be better?

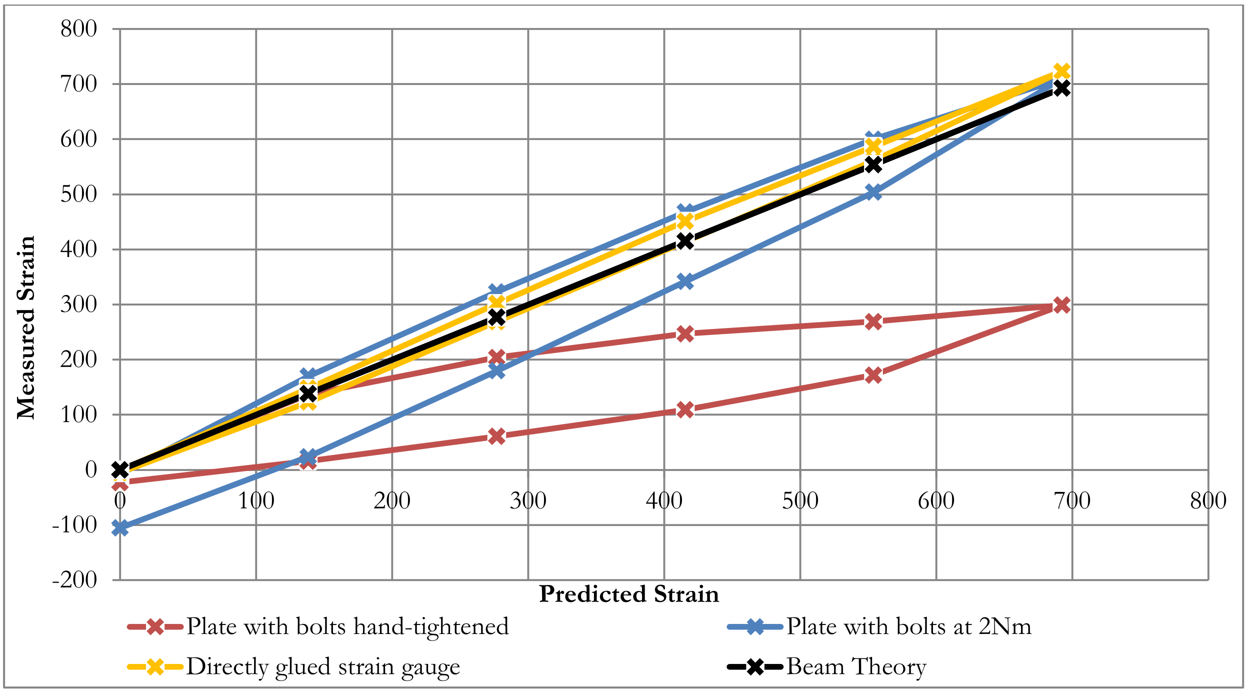

Figure 5.6: Original plate design tests in tension

The experiments were re-run with larger M4 bolts used (instead of M3), which were capable of transferring a torque of 4Nm. The results of these experiments are displayed in Figure 5.7, and show that increasing the torque to 4Nm results in an even greater linearity in the strain readings. The results are also closer to returning to 0 than the results from the 2Nm torque tests (these are shown in Figure 5.7 too, for comparison). However, the magnitude of the readings from the 4Nm tests are higher than that of the beam theory predictions. At this stage, the main area of interest is the linearity and repeatability of the readings.

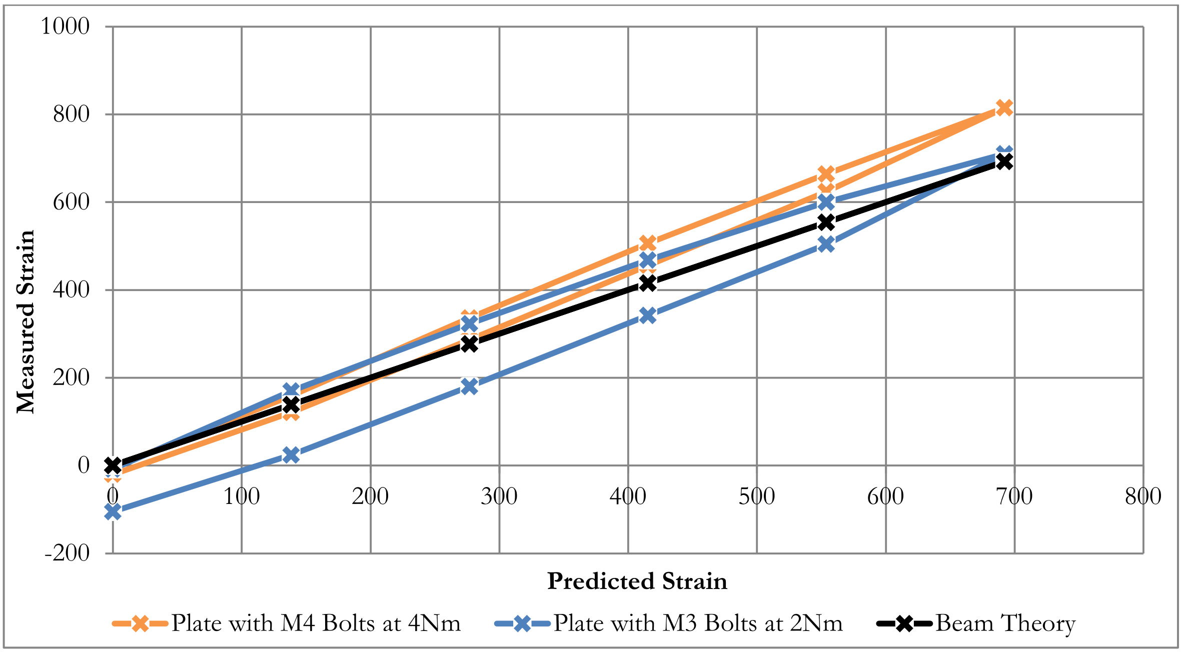

Figure 5.7: Results with the original plate design using M4 bolts, which are compared with M3 bolts (in tension)

5.4.2 Compression Results

The results of the initial compression experiments are shown below in Figure 5.8. The results show that the plate buckles at around -400 microstrains. Buckling does not appear to have happened to the plates installed at TCR, most likely because the soil load was acting on the plate to prevent outwards buckling, and the timber prevents inward buckling. However, this behaviour of the plate should be investigated. Therefore, these results led to a redesign of the plate, to try and prevent buckling in compression, and also improve tension results.

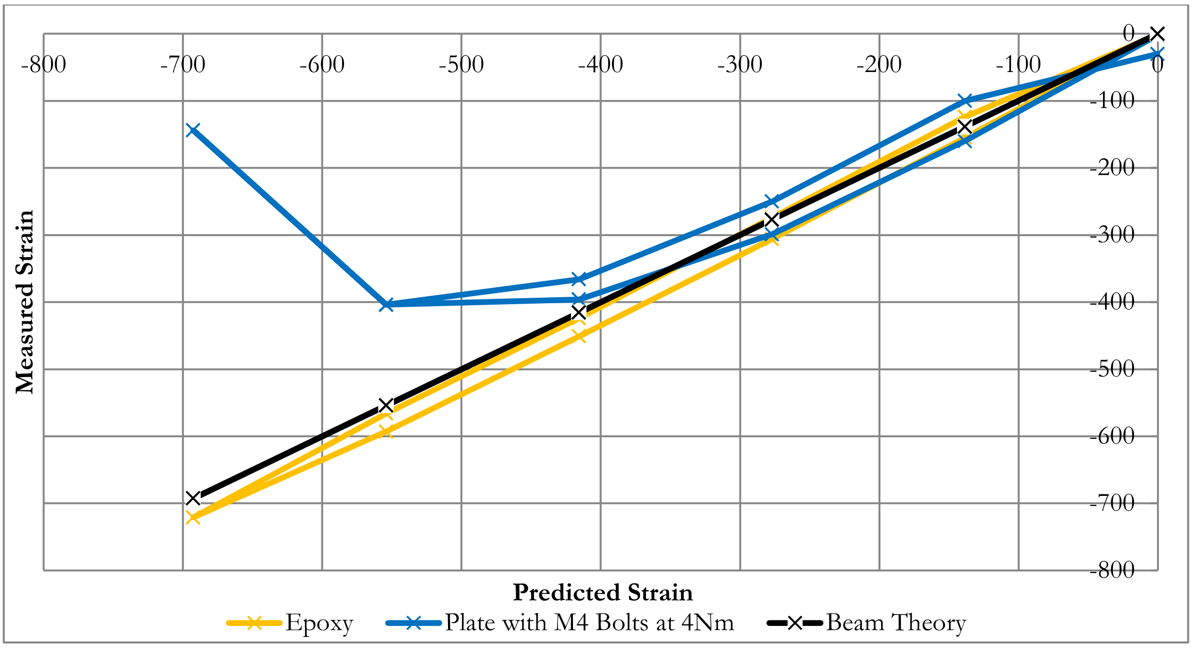

Figure 5.8: Compression results for the original plate design, with M4 bolts at 4 Nm

5.5 Strain Monitoring of Timber Structures: Literature Review

Prior to embarking on a new design, gathering information about other designs in literature was intended to suggest any possibilities that had not yet been considered. This research found that methods of monitoring strain in timber (using foil gauges) are not well documented, and that authors have had similar issues in the past.

5.5.1 Methods of Strain Gauge Attachment

5.5.1.1 Shoef & Shoef (2006)

One paper has been found which reports methods of attaching strain gauges using a plate-like device. Shoef & Shoef (2006), monitored crack propagations in a masonry structure during the relocation of a C19th German Temple Society building in Palestine. Although these gauges were attached to masonry, the methods of attachment are very similar to the plate attachment used in this project. It is observed in Figure 5.9 that both the methods of attachment used by Shoef & Shoef elevate the strain gauges from the surface being monitored, and large bolts were used. Data was collected using a datalogger.

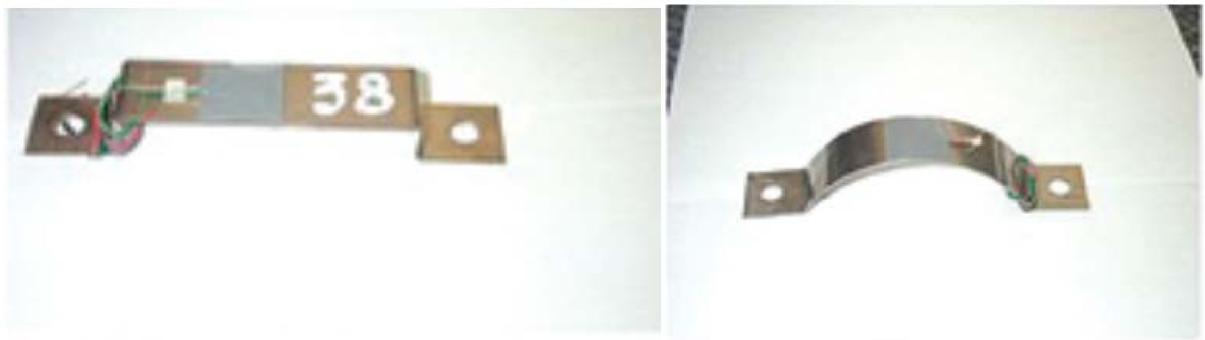

(a) **(b)**
Figure 5.9: (a): rounded bracket; (b): straight bracket (Shoef & Shoef 2006)

Also of interest is their method for calibrating the attachment brackets. They developed a device which deforms the brackets to a known elongation, which calibrates the output from the strain gauges (see Figure 5.10). Shoef & Shoef report that their strain gauges could accurately detect a minimum deflection of 0.01mm, which is the same resolution used in the SmartPlank calibration (the central dial gauge is 100div/mm). Their method of attaining these results was by using the calibration device, whereas for the SmartPlank project a loaded beam is used. The method of calibration used in this project, a 4-point bending platform, is a much bigger device, and should therefore have a smaller error in calibration.

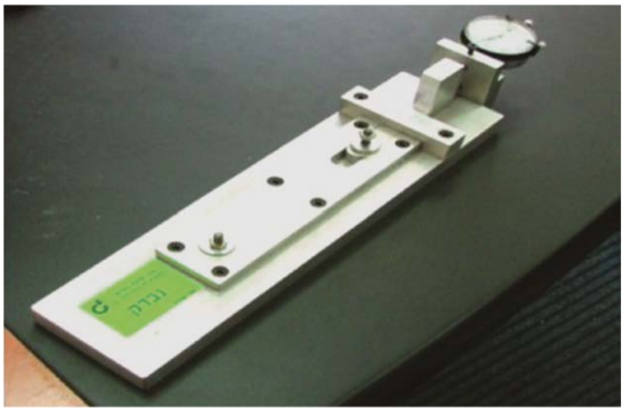

Figure 5.10: Calibration device (Shoef & Shoef 2006)

5.5.1.2 Others

Hale & Chapman (2014) report on strain monitoring in a timber windmill. Having never monitored strain in timber before, and unable to find helpful literature, they turned to Vishay Measurements Group for advice. Their conclusion was to use adhesive to fix strain gauges to timber. This is generally the case for any other literature found, e.g., Jankowski et al. (2010).

5.5.2 CUED Structures Research Lab

The foil gauge based method for measuring strain in the structures lab is to use a portal frame, as shown Figure 5.11(a). This is a device which is 100mm in length, with two spikes at each end. The spikes are inserted into small holes (which are fixed in place in the material being monitored) and held in place with springs (or elastic bands). The portal frame is calibrated in a device (shown in Figure 5.11(b)) which can measure precisely the distance between the two spikes, whilst the strain is being monitored. This device is considered to accurately measure strain and is widely used within the structures lab. It can also be set up to measure displacement.

(a) **(b)**

Figure 5.11: (a): CUED structures lab portal frame; (b): CUED structures lab calibration device

5.5.3 Summary

It has been found that in the limited literature available, strain gauges are attached to timber using adhesive. However, results from the SmartPlank project have recently been encouraging. Testing on a steel beam has shown that a cause for erroneous readings is the torque in the bolts which attach the plate. This seems to agree with Shoef & Shoef, who used quite large bolts with their bracket designs (which is the most relevant research found relating to this project).

Considering the differences between the plates used by Shoef & Shoef, and the current plate design for this project, it is difficult to see why one may be better than the other. Shoef & Shoef used their plates to measure simple linear displacement in masonry, rather than bending strain in timber. Although they report good results, it is not necessarily the case that their design would perform equally well in bending. Given that results discussed in section 6.4 show promising improvements in readings from the current design, it was decided to continue pursuing the current plate design for this project.

5.6 Reconsidering Plate Design

A simple buckling calculation can be made, by considering the maximum compressive strain that the plate attachment is likely to endure, as shown below in Figure 5.12.

Figure 5.12: Schematic of forces induced in plates due to bending of the beam

Assuming that the maximum induced strain is 2000µε (as seen at SmartPlank no.52, at Tottenham Court Road, shown in Figure 5.13):

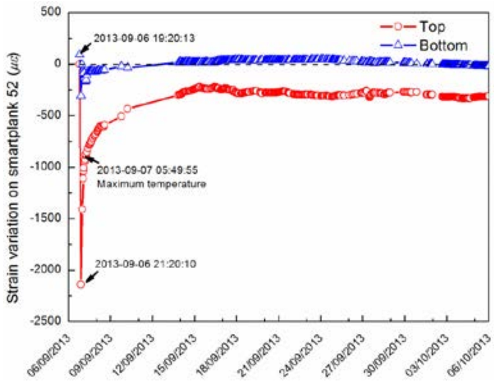

Figure 5.13: Results from a SmartPlank installation at TCR (Xu et al. 2015)

the maximum force (F_c in Figure 5.12) is therefore:

$$F_c = \varepsilon EA = (2000 \times 10^{-6})(70 \times 10^{3})(20 \times 0.5) = 1.4kN$$

Where E=70GPa, and the width and thickness of the plate are 20mm and 0.5mm respectively. Now, from experimental results it has been observed that buckling actually occurs in this plate at 400µε (see Figure 5.8), thus the observed bucking load is

$$F_{c,observed} = \varepsilon EA = (400 \times 10^{-6})(70 \times 10^{3})(20 \times 0.5) = 0.28kN$$

The buckling deformation is hypothesised as shown in Figure 5.14:

Figure 5.14: Hypothesis of buckling deformation for plate

with effective length equal to 0.5 times the length; and therefore the theoretical buckling load of the current design can be estimated using the standard Euler Buckling equation:

$$P_E = 4\pi^2 \frac{EI}{l^2} = \frac{4\pi^2 \times 70 \times 10^3 \times \frac{20 \times 0.5^2}{12}}{40^2} = 0.35kN$$

Thus for the purposes of this design a safety factor of at least $\frac{P_E}{F_{c,observed}} = \frac{0.35}{0.28} = 1.25$ is required. A summary of the options considered is shown in table 7.1:

Option	Length (mm)	Thickness (mm)	F_c maximum (kN)	Theoretical P_E (kN)	Safety Factor
1	16.6	0.5	1.4	2.1	1.5
2	30	1	2.8	5.1	1.825
3	25	1	2.8	7.4	2.6

Table 5.1: The main design options considered

It was considered that option 1 would not leave enough space for the strain gauge to read a region of constant strain, since at the point where the sides of the plate meet the thin region, there is likely to be a stress concentration, which may affect the way that strain develops across the thin region where the strain gauge is located (as shown below in Figure 5.15).

Figure 5.15: Schematic of a shorter plate, showing the size of the strain compared to the plate (to scale)

Therefore, option 2 was considered the most practical. Now, given the results from testing of the original design, it was found that the greater the torque in the fixings the better the readings, but the current bolts (M3) can only transfer up to 2Nm of torque (in steel). After discussions with Neil Houghton (Senior Design Engineer in the CEUD), it was hypothesised that a torque of around 4Nm would be required (using a simple F=μR calculation), in order to develop enough friction between the plate and the beam below, to prevent slipping of the plate. To achieve this torque, for connecting aluminium to steel, M4 bolts are required (from the Unbrako

Hexagon Socket Screws Technical Data Booklet). The new design for testing on a steel beam is shown below, in Figure 5.16.

Figure 5.16: Design of the plate for testing on a steel beam

Data for torque induced by screws in timber is not available. However, the lateral capacity of the screws can be found in Eurocode 5 (IStructE & TRADA 2007). From Eurocode 5, one 6mm screw can laterally carry 2.17kN. Thus, with two screws on each side of the plate, around 4.7kN could be carried laterally. This provides a lateral safety factor of 1.55 (=4.7/2.8).

In addition, for these screws to be used in timber, they need to be a certain spacing apart, so that the timber is not damaged by the screws being too close to each other. According to Eurocode 5, table 6.11, the minimum spacing required for wood screws is 4 times the diameter. Thus the spacing required is at least 24mm (as shown in Figure 5.17, for the final timber design).

Despite Eurocode 5 being for use in the design of structures, it is considered that because of this, that its application to this design process should be conservative, and that therefore the potential damage to the timber should cause as little disturbance to strain measurement as possible.

Figure 5.17: Design of the plate for testing on a timber beam

5.7 Results and Discussion of New Designs

The new design was initially tested on steel, and the effect of varying the torque in the bolts was investigated. The plate was then tested on timber.

5.7.1 Torque Investigation

The torque applied to the bolts, for the plate tested on steel, was varied using a torque meter. The M4 bolts could carry up to 4Nm of torque, so the experiments were repeated at 1Nm, 2Nm, 3Nm and 4Nm of torque in the bolts. The results are shown below in Figure 5.18. When the bolts were tightened to 1Nm, the readings were very non-linear. It can be seen that linearity increases with increasing torque in the bolts. The hysteresis of the readings also reduces with increased torque, as seen by the smaller vertical distances between readings during loading, and readings during unloading (of the same predicted strain). From these observations, it appears that 4Nm of torque provides the best readings.

However, at higher strains, the readings closest to beam theory predictions are provided by the bolts tightened to 2Nm, although at lower strains, the readings closest to beam theory predictions are provided by bolts tightened to 4Nm. Despite this, it is concluded that 4Nm of torque provides the most reliable readings, due to the greatest linearity and smallest hysteresis, as hypothesised in design (section 6.6). It is expected that greater torque improves readings, because this provides a greater friction between the plate and the beam.

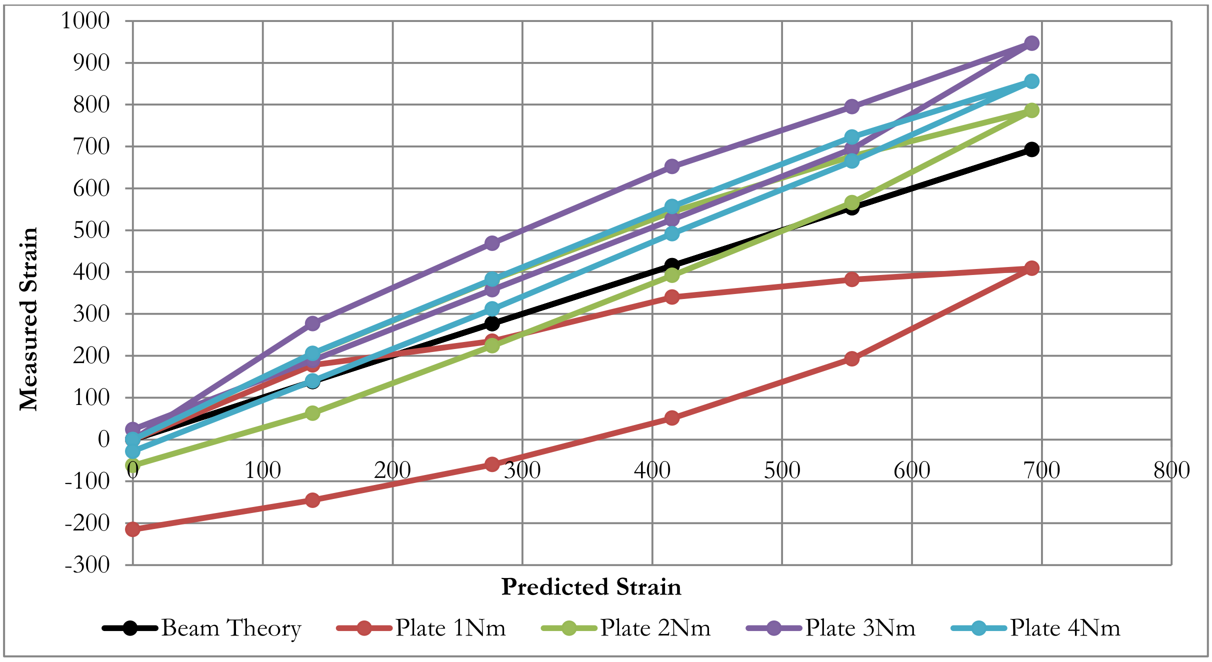

Figure 5.18: Tensile performance of the new plate design, with varying torque in the M4 bolts (on steel beam).

5.7.2 Compression Results

Compared to readings from the previous plate design, which was 0.5mm thick, the 1mm thick plate readings are greatly improved, and the plate no longer buckles at 400με (as shown by Figure 5.19). The readings during loading are very linear (although quite a lot larger than beam theory predictions). In addition, the readings jump up unexpectedly at around 200με. This might be due to deformation of the plate pushing it against the beam. Therefore, this plate would be useful for a rough indication of compressive strain, but is not as accurate as when used in tension.

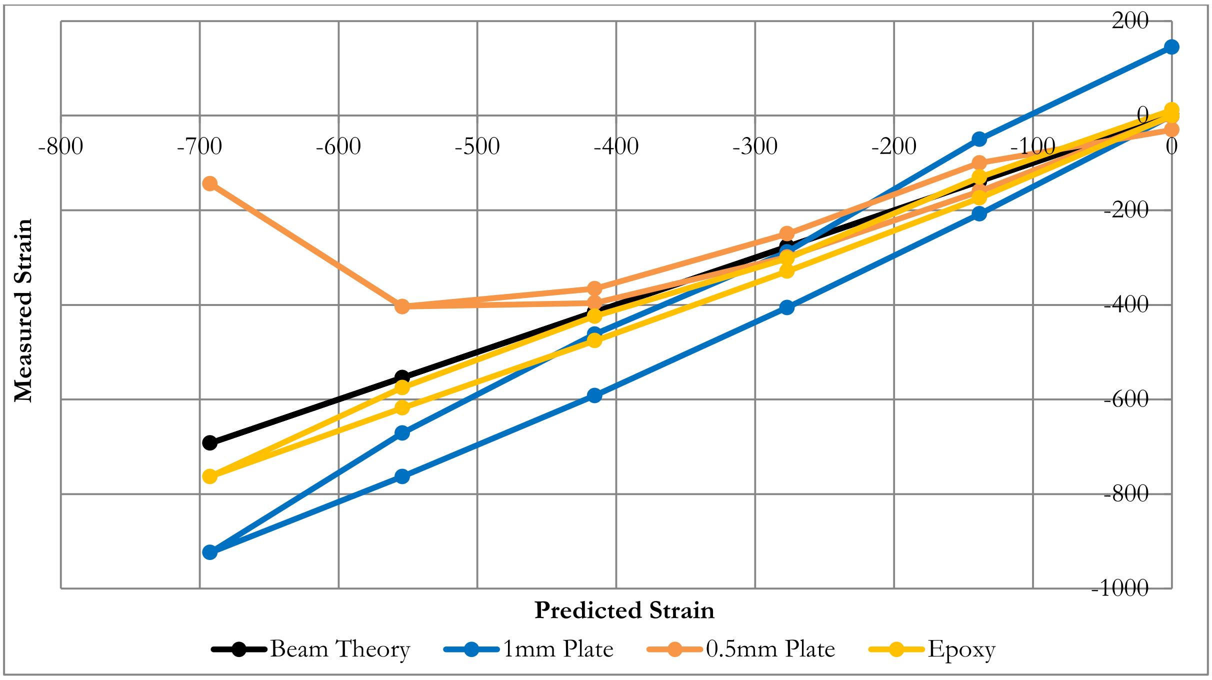

Figure 5.19: Compressive performance of new plate (1mm thick) compared to the old plate (0.5mm thick)

5.7.3 Performance on Timber

The results from the timber experiment in tension are shown in Figure 5.20. It can be seen that there is much less linearity of both the epoxy and the plate results, compared with the steel experiments. In addition, the magnitudes of both are less accurate. The magnitude of the plate attachment is significantly less than beam theory.

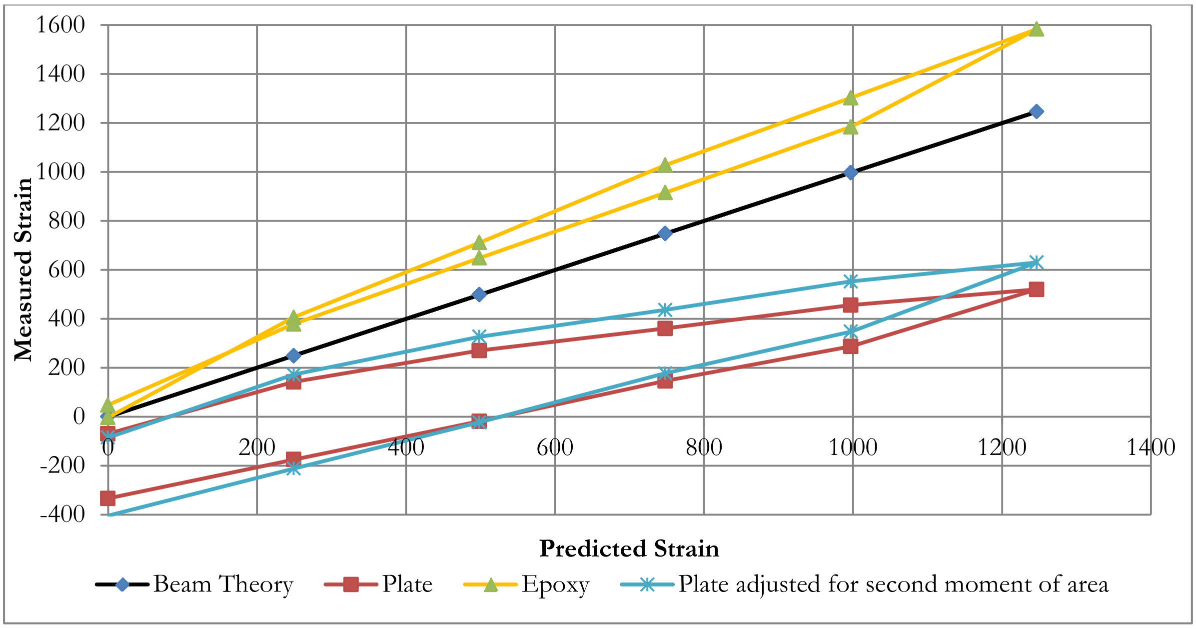

Figure 5.20: Timber results in tension

The timber used was stock timber (not graded) from Ridgeons, with dimensions 45mm by 45mm. This means that the plate was a similar size to the width of the beam, and the wood screws used penetrated around half of the depth of the beam. Figure 5.21 shows how the variation of strain within the beam raises the question of what part of the screw provides fixity for the plate, given that the strain varies from maximum tensile strain to zero (and possibly some compression), along the length of the screw.

Figure 5.21: Variation of strain along the length of the wood screw. Note: vertically to scale for this experiment, however bending is exaggerated.

A major assumption described in section 5.2 is that the stiffness of the plate does not influence the stiffness of the timber beam. This was made because the Young's Modulus (E) and the yield strength of aluminium alloy 6028 were assumed to be comparable to that of timber. In reality, the E values will be quite different. Therefore, considering this assumption more carefully, a calculation can be made to investigate the expected differences. A transformed second moment of area of the section can be estimated, and therefore how the strain developed is influenced. Figure 5.22 shows how the cross section through the timber beam and the centre of the plate, can be analysed using a simple material conversion to estimate the second moment of area.

Figure 5.22: Section through the timber beam and the centre of the plate; used for calculating change in second moment of area

The Young's Modulus of the plate is 70GPa (for aluminium alloy 6028) and assumed to be 9GPa for the timber (as stated in the CUED structures databook), yields that the second moment of area is increased by approximately 21.2%. Since $\varepsilon = \frac{My}{EI}$, this means that the strain in the timber will be approximately 82.5% of the expected value. This adjusted strain value is shown in Figure 5.20, which shows that this has little effect on the overall error. It is therefore concluded that the main driver of the results is the fixity of the screws. The results shown in Figure 5.20 suggest that the screws act as if they are fixed at a point quite below the surface. Tests on a larger beam could confirm this.

Ideally this experiment would have been repeated using a full scale beam in the structures lab, especially since the results from the epoxy gauge are not as good as expected. However there was unfortunately not enough time to carry out all of the experiments planned for (described in the *Technical Milestone Report*).

5.8 Further Designs

This current plate design requires more comprehensive testing, on a full scale beam. It is hoped that with further testing and design tweaks, the behaviour of the plate can be improved and better understood. There is another design being considered, which is currently showing promising results in the CSIC lab. A plywood prototype is shown in Figure 5.23, compared with the current design.

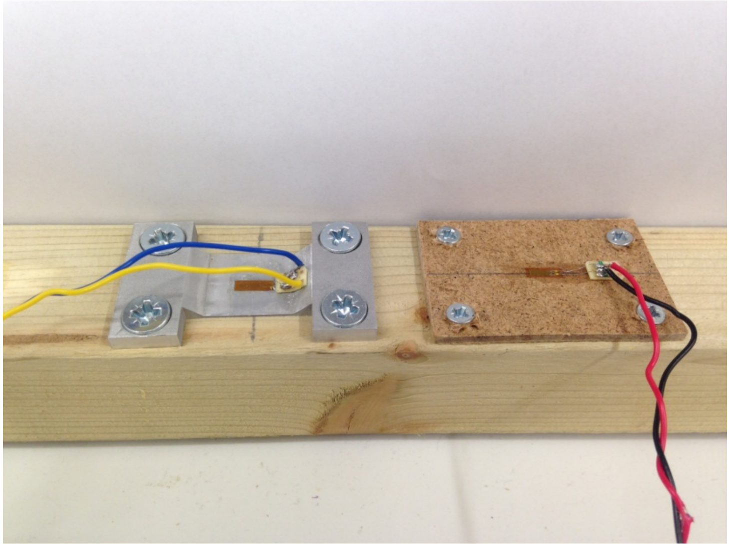

Figure 5.23: A prototype design (right) being developed in the CSIC, compared with the design evaluated in this report (left)

6 Conclusions

1. The finite element model developed in Strand7 has produced encouraging results, which combined with measurements from a previous strain gauge plate attachment design, indicate that the design loads for the timber beams used in TCR may be greatly over estimated.
2. It is possible that grouting is more crucial for design than overburden pressure.
3. The performance of the strain gauge plate attachment has been investigated, and a new design has been developed, which has shown some promising results when tested on a steel beam. Its performance on timber has been less promising.
4. Therefore further work is required to investigate the performance of the strain gauge plate attachment on timber. However, it is hypothesised that testing on a full-scale beam could yield better, more informative results.
5. Once the method of SmartPlank measuring strain in the timber is fully verified, confidence in [1] and [2] will start to allow discussion regarding design methods.
6. The Strand7 model could be further developed to account for more detailed aspects of the tunnel design, such as horizontal pressure provided by surrounding soil, and any irregular aspects of particular supports.
7. It is certainly the case that further developments in SmartPlank, combined with finite elements models such as the one developed in the course of this project, will lead to a greater understanding of the behaviour in timbers in underground construction.

7 Future Work

The main areas of future work identified are:

1. Further experiments of the strain gauge plate attachment on a full scale timber beam
2. Investigation of different materials used to attach strain gauges (such as plywood)
3. Adapting the Strand7 model to analyse future SmartPlank installations

8 Risk Assessment Retrospective

The initial risk assessment was written prior to full knowledge of all the experimental work that would be carried out. However, all the experimental work went well, with little exposure to risks. A site visit to TCR was fully prepared for by the contractor, and site inductions and health and safety inductions were carried out, and all the necessary PPE was provided.

If an experiment, or some work, were needed to be carried out which had a new risk highlighted, it may have been sensible to update the risk assessment. For example, when fixing strain gauges to the plate attachments, superglue and acetone were used, and a soldering iron. These were all used under the supervision of Peter Knott (CSIC Senior Technician), but perhaps his supervision may not have been as necessary with a more comprehensive risk assessment.

9 Acknowledgements

The author would like to that the following for their help, ideas, and patience throughout this project: Dr Xiaomin Xu, Professor Kenichi Soga, Matthew Wilcock, Peter Knott, Alistair Ross, Krishna Kumar and Martin Touhey.

10 References

Aslte, P. et al., 2013. Conceptual Design Statement for Central Line Stair 14 Temporary Works (Phase 1). *OTB Engineering*.

Cheuk, D., 2012. *4th Year Final Report*.

Daehnke, A. et al., 2000. The impact of soft loading conditions on the performance of elongate support elements. *CSIR: Divison of Mining Technology*.

Hale, J.M. & Chapman, M.M., 2014. Design, Installation and Calibration of a Strain Gauge Structural Monitoring System for a Timber Windmill. *Experimental Techniques*, 38(3), pp.45–53. Available at: http://doi.wiley.com/10.1111/j.1747-1567.2011.00801.x.

IStructE & TRADA, 2007. Manual for the Design of Timber Building Structures to Eurocode 5.

Jankowski, L.J., Jasieńko, J. & Nowak, T.P., 2010. Experimental assessment of CFRP reinforced wooden beams by 4-point bending tests and photoelastic coating technique. *Materials and Structures*, 43(1-2), pp.141–150.

Mackenzie, C.N.P., 2014. Traditional Timbering in Soft Ground Tunnelling, A Historical Review. *The British Tunnelling Society*.

Ryder, J. a & Jager, a J., 1995. The design of pillar systems as practised in shallow hard-rock tabular mines in South Africa. *Journal of the South African Institute of Mining and Metallurgy*, (February), pp.7–18.

Shoef, G. & Shoef, Y., 2006. Structural health monitoring at a displacement project. *Insight: Non-Destructive Testing and Condition Monitoring*, 48(3), pp.178–180.

Xu, X. et al., 2015. Performance monitoring of timber structures in underground construction using wireless SmartPlank. *Smart Structures and Systems*, 15(3), pp.769–785.